



Shifts in the Ediacaran to Lower Ordovician sedimentary zircon provenances of Northwest Gondwana: the Pyrenean files

Maxime Padel, Sébastien Clausen, Marc Poujol, Jose Javier Alvaro Blasco

► To cite this version:

Maxime Padel, Sébastien Clausen, Marc Poujol, Jose Javier Alvaro Blasco. Shifts in the Ediacaran to Lower Ordovician sedimentary zircon provenances of Northwest Gondwana: the Pyrenean files. *Geologica Acta*, 2022, 20, pp.1 - 18. 10.1344/geologicaacta2022.20.14 . insu-03843473v2

HAL Id: insu-03843473

<https://insu.hal.science/insu-03843473v2>

Submitted on 7 Dec 2022

HAL is a multi-disciplinary open access archive for the deposit and dissemination of scientific research documents, whether they are published or not. The documents may come from teaching and research institutions in France or abroad, or from public or private research centers.

L'archive ouverte pluridisciplinaire **HAL**, est destinée au dépôt et à la diffusion de documents scientifiques de niveau recherche, publiés ou non, émanant des établissements d'enseignement et de recherche français ou étrangers, des laboratoires publics ou privés.



Distributed under a Creative Commons Attribution - ShareAlike 4.0 International License

Shifts in the Ediacaran to Lower Ordovician sedimentary zircon provenances of Northwest Gondwana: the Pyrenean files

Maxime Padel¹ Sébastien Clausen² Marc Poujol³ J. Javier Álvaro⁴

¹Bureau de Recherche Géologique et Minière (BRGM), Direction des Géoressources (DGR), BP36009
45060 Orléans E-mail: m.padel@brgm.fr

²University of Lille, Centre National de la Recherche Scientifique (CNRS), Unité Mixte de Recherche (UMR) 8198 - Evo-Eco-Paleo
F-59000 Lille, France. E-mail: sebastien.clausen@univ-lille1.fr

³University of Rennes, CNRS, Géosciences Rennes
UMR 6118, 35000 Rennes, France. E-mail: marc.poujol@univ-rennes1.fr

⁴Instituto de Geociencias (CSIC-UCM)
Dr. Severo Ochoa 7, 28040 Madrid, Spain. E-mail: jj.alvaro@csic.es

ABSTRACT

Detrital zircon grains from Cambrian–Lower Ordovician sandstones and quartzites sampled in the Pyrenees were dated by LA-ICPMS in order to assess their provenance sources. Resulting age distributions are compared to other available datasets from neighbouring margins, such as Morocco, the Iberian Peninsula, southern France and Sardinia. Kolmogorov-Smirnov (K-S) test and Crystallization Age-Depositional Age (CA-DA) diagrams were used to compare zircon populations estimating their possible correlation with the arc/rift/drift geodynamic evolution of the northwestern Gondwana margin. During Terreneuvian times, zircon populations allowed the distinction of i) a southwesternmost edge (Atlas-Ossa-Morena Rift) mostly influenced by Panafrican and Anti-Atlasian sources (ca. 0.63–0.54), ii) a northeasternmost edge (Sardinia) recording the influence of the Saharan Metacraton and the Arabian Nubian Shield, with a distinct Stenian–Tonian shift (ca. 1.25–0.85Ga) and iii) an intermediate palaeogeographic transect, where lies the Central Iberian, West Asturian-Leonese and Cantabrian Zones, the Montagne Noire and the Pyrenees sharing similar populations and a chronologically progressive influence from Anti-Atlasian/Panafrican to Saharan Metacraton/Arabian Nubian Shield sources. This gradual modification in zircon percentage populations supports similar trends based on climatically sensitive indicators, biogeographic patterns of Cambrian Epoch 2 archaeocyathan and microfossil assemblages, and laterally correlatable episodes of carbonate production, all of them pointing to a Cambrian setting for the Pyrenean Basin between the Montagne Noire (Occitan Domain) and the Sardinian margins of NW Gondwana. The Terreneuvian zircon patterns recorded in the Pyrenees gradually evolved from Cambrian Epoch 2 to Early Ordovician times, reflecting the geodynamic evolution from Panafrican and Cadomian arc-related to rift-dominant conditions. During Furongian and Ordovician times, the relative percentage of zircon populations led to a more spread age curve, characteristic of extensional settings and pointing to rift (passive margin) conditions.

KEYWORDS Orogeny. Rift. Palaeogeography. Pyrenees. Detrital zircon. Gondwana.

INTRODUCTION

Detrital zircon U-Pb geochronology is a powerful tool to characterize crustal growth episodes, deciphering detrital sources, estimating the maximum depositional age of strata, and constraining the geodynamic evolution of continental margins (e.g. Gehrels, 2014). During the two last decades, the analysis of zircon provenances has been regularly applied to identify the different sources of the Neoproterozoic–early Palaeozoic basins fringing Northwest Gondwana in order to determine their relative proximity to different orogens (e.g. Altumi *et al.*, 2013; Avigad *et al.*, 2012, 2018; Ballouard *et al.*, 2018; Couzinié *et al.*, 2019; Drost *et al.*, 2011; Fernández-Suárez *et al.*, 2014; Gutiérrez-Alonso *et al.*, 2003; Kydonakis *et al.*, 2014; Linnemann *et al.*, 2008; Margalef *et al.*, 2016; Meinhold *et al.*, 2011, 2013; Padel *et al.*, 2017a,b, 2018; Pastor-Galán *et al.*, 2013; Shaw *et al.*, 2014). Among these orogenic events, the Neoproterozoic Panafrican (Anti-Atlas, 790–560 Ma), Cadomian (e.g. Armorican Massif, Iberia and Bohemian Massif, 850–550 Ma) and Avalonian (e.g. Newfoundland, New England, Nova Scotia and Cape Breton, 730–570 Ma) events have received particular attention as they share a broad shift from convergent to extensional conditions, with a turnover close to the Ediacaran–Cambrian boundary interval (590–540 Ma; Ballèvre *et al.*, 2001; Blein *et al.*, 2014a, b; Linnemann *et al.*, 2007; Murphy *et al.*, 1999; Nance *et al.*, 2002; Stampfli and von Raumer, 2008; Stampfli *et al.*, 2013).

In NW Gondwana (including the Moroccan Anti-Atlas, the Iberian Peninsula, southern France and Sardinia), evidences for this arc/rift geodynamic change are preserved in disconnected basement exposures of the European Variscan Belt (Fig. 1A). In southwestern Europe, the Variscan Ibero-Armorican Arc contains two branches (Ballèvre *et al.*, 2009; Martínez Catalán *et al.*, 2007; Pouplet *et al.*, 2017): i) a southwestern branch represented by the Iberian Massif and ii) a northeastern branch that includes the Armorican Massif, the South Armorican Domain (southwestern Britany and Vendée), the northern Massif Central, the Occitan Domain (Albigeois, Montagne Noire, Mouthoumet, and Cévennes massifs of the southern Massif Central) and its lateral prolongation into the Pyrenean Domain, Corsica and Sardinia. Although the Pyrenees share strong Ediacaran–Cambrian stratigraphic similarities with the Cantabrian Zone, the Montagne Noire and SW Sardinia, its Cambrian palaeogeographic position has been an everlasting matter of discussion (Álvaro *et al.*, 2014a; Ballèvre *et al.*, 2009; Laumonier *et al.*, 1996, 2004; Pouplet *et al.*, 2017). As a result, the palaeogeographic position of the Pyrenees is often questioned or even omitted in many Ediacaran–early Palaeozoic palaeogeographic reconstructions of Gondwana (e.g. Murphy *et al.*, 2004; Nance *et al.*, 2008).

This study aims to assess the evolution, across space and time, of the influence of sedimentary zircon populations during Cambrian–Early Ordovician times throughout a palaeogeographic SW-NE transect of NW Gondwana. It focuses on successions from the Anti-Atlas (Morocco), the Ossa-Morena, Central Iberian, West Asturian-Leonese and Cantabrian Zones of the Iberian Massif, the central and eastern Pyrenees (France/Spain border), the Montagne Noire (France) and southern Sardinia (Italy). We present here a comprehensive study of detrital zircon grains from Cambrian sandstones and quartzites in the Pyrenees, completed with other Ediacaran and Ordovician samples from the Pyrenees analysed by Casas *et al.* (2015), Margalef *et al.* (2016) and Padel *et al.* (2018). Our study is based on a multi-tool analysis of Kernel density plots (KDE), statistical Kolmogorov-Smirnov (K-S) tests and Crystallization Age-Depositional Age (CA-DA) diagrams, which leads to the proposal of new palaeogeographic constraints for the geodynamic evolution of NW Gondwana during Ediacaran to Ordovician times.

GEOLOGICAL SETTING AND STRATIGRAPHY OF THE PYRENEES

The basement of south-western Europe includes, among others, the core of the Iberian and Armorican massifs, the French Massif Central and the Pyrenees. Recent palaeogeographic re-appraisals based on litho- (Padel *et al.*, 2018) and biostratigraphic revisions (Wallet *et al.*, 2022), completed with correlations of the mid-Ordovician Sardic Phase (Álvaro *et al.*, 2020 and references within) have placed the Ediacaran–Ordovician Pyrenean margin of Gondwana as a lateral continuity of neighbouring domains, such as the Occitan Domain (including Montagne Noire and the Mouthoumet massifs) and SW Sardinia. As a result, the Cambrian Pyrenean Basin has been recently integrated in the reconstruction of pre-Variscan palaeogeographic puzzles along NW Gondwana, after combining structural, magmatic and stratigraphic comparisons (e.g. Álvaro *et al.*, 2021; Casas and Murphy, 2018).

The present-day Pyrenean Belt formed as an intracontinental fold and thrust belt related to a Late Cretaceous to Early Neogene collision between the Iberian microplate and the southern European plate. The belt is subdivided into three E–W morphostructural units, the Northern, Axial and Southern zones (Barnolas and Chiron, 1996). The Axial Zone consists of a complete Ediacaran to Carboniferous succession intruded by Ordovician granites, which include distinct migmatized orthogneiss aureoles, and Variscan anatexitic granites (Casas *et al.*, 2010; Castiñeiras *et al.*, 2008; Cocherie *et al.*, 2005; Deloule *et al.*, 2002; Denèle *et al.*, 2009; Lemirre *et al.*, 2019; Liesa *et al.*, 2011; Martínez *et al.*, 2011; Mezger and Gerdes, 2016).

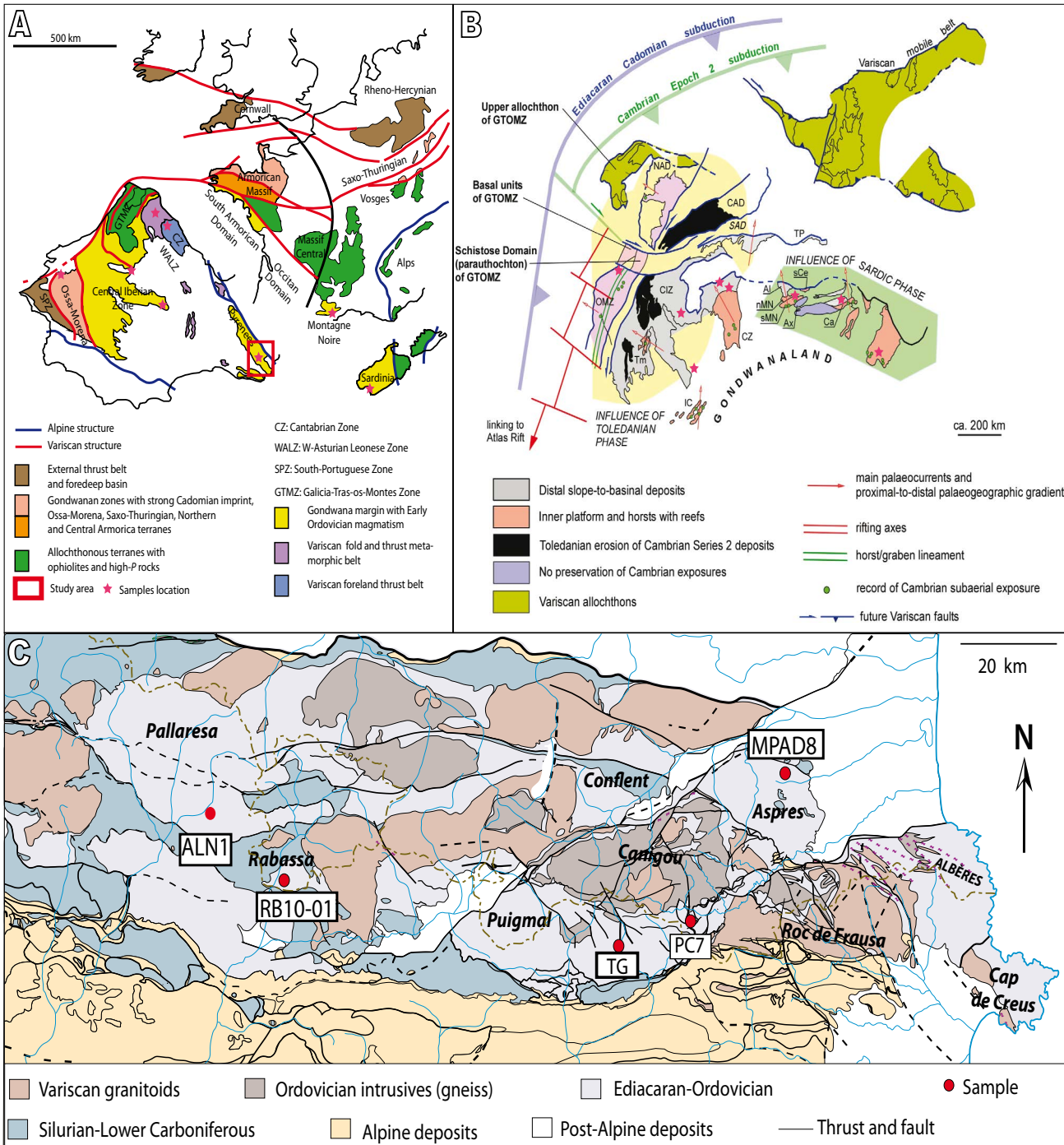


FIGURE 1. A) Geological sketch of the Variscan Belt in southwestern Europe with tectonostratigraphic domains including Cambrian–Ordovician exposures from peri-Gondwana; modified after Ballèvre *et al.* (2009), Martínez-Catalán (2007) and Poulet *et al.* (2017). B) Early Palaeozoic palaeogeographic reconstruction of different basement domains in SW Europe, based on Álvaro *et al.* (2021). Al= Albigeois Mountains; Ax= Montagne Noire Axial Zone; Ca= Canigó Massif; CAD= Central Armorican Domain; CIZ= Central Iberian Zone; CZ= Cantabrian Zone; GTOMZ= Galicia-Trás-os-Montes Zone; IC= Iberian Chains; NAD= North Armorican Domain; nMN= northern Montagne Noire; OMZ= Ossa-Morena Zone; sCé= southern Cévennes; sMN= southern Montagne Noire; Tm= Toledo Mountains. C) Geological map of the eastern Pyrenees (Red squared in A) with setting of studied samples; modified after Padel *et al.* (2018).

The metamorphic domes resulting from the Variscan orogeny are surrounded by various metamorphic grades affecting the entire pre-Variscan strata (e.g. Cochelin *et al.*,

2018; Fig. 1C). The Axial Zone is bounded by the North- and South-Pyrenean Thrusts (Laumonier *et al.*, 2015), subsequently flanked by post-Variscan-dominant series.

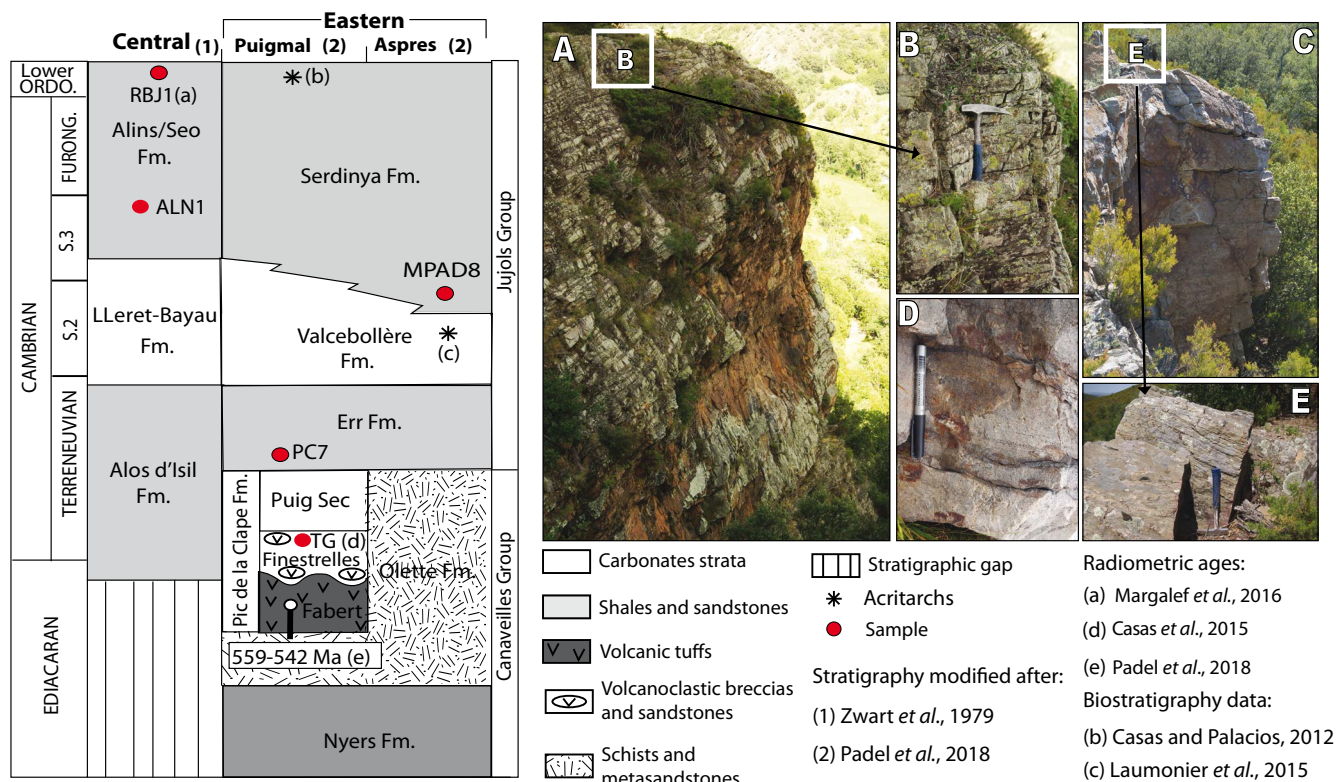


FIGURE 2. Ediacaran–Lower Ordovician stratigraphic chart of the central and eastern Pyrenees with locations of studied samples (red circles). A) Picture with location of the meta-sandstone where sample ALN1 was extracted. B) Zoom on the location of sample ALN1. C) Picture with location of the meta-sandstone where sample MPAD8 was extracted. D) Picture of the meta-sandstone where sample PC7 was selected. E) Detail of the location of sample MPAD8.

Pre-Variscan rocks mostly crop out in the central and eastern Axial Zone, from the Pallaresa Dome to the Mediterranean Sea (Fig. 1C). In the eastern Pyrenees, several tectonostratigraphic units are recognized, such as the Puigmal, Conflent, Aspres, Roc de Frausa, Albera and Cap de Creus units (Fig. 1C). Their Ediacaran–Lower Ordovician succession is subdivided into the Canaveilles and Jujols groups (Laumonier et al., 1996, 2004; Padel et al., 2018; Fig. 2). The Ediacaran Canaveilles Group, 2–3km thick, is a monotonous micaschist-dominant succession locally punctuated by rhyolites, volcanosedimentary breccias, marbles and quartzites. The presence/absence of carbonate interbeds allows deciphering between the (lower) Nyers and the (upper) Olette formations. The latter is capped, in the Puigmal tectonostratigraphic unit (Padel et al., 2018) (Fig. 2), by a volcanosedimentary complex, up to 500m in thickness, named Pic de la Clape Formation, where three members have been distinguished: i) the Fabert Member, a succession of bedded metarhyolites, up to 50m thick, interbedded with intraformational breccias, arkoses, shales and basic lava flow interbeds; ii) the Finestrelles Member, a package of massive felsic-dominant ignimbrites and volcanosedimentary breccias, up to 500m thick, interbedded with tuffaceous sandstones and siltstones, and

locally punctuated by pristine-to-volcaniclastic limestone interbeds and iii) the Pic de la Clape Formation, up to 180m thick, composed of massive to bedded limestones and marbles (Padel et al., 2018). The overlying Miaolingian–Lower Ordovician Jujols Group has an estimated thickness of 3–4km and comprises, from bottom to top, the Err, Valcebollère and Serdinya formations. The Err Formation, ~1500m thick, consists of shale/metasediment alternations, conformably overlain by the massive to bedded limestones and marbles of the Valcebollère Formation, 200–300m thick. Finally, the Serdinya Formation, ~2000m thick, consists of homogeneous micaschists and shales, irregularly punctuated by centimetre to decimetre-thick sandstone interbeds (Casas and Palacios, 2012).

In the Pallaresa dome of the central Pyrenees, a thick (>4000m) siliciclastic-dominant succession can be subdivided into three units, named the Alos d’Isil, Lleret-Bayau and Alins formations (Laumonier et al., 1996), which represent the three-fold subdivision of the Jujols Group reported above. In the Rabassa Unit, the same succession is represented by the Seo Formation, a lithostratigraphic equivalent to both the Serdinya and Alins Formations (Figs. 1; 2).

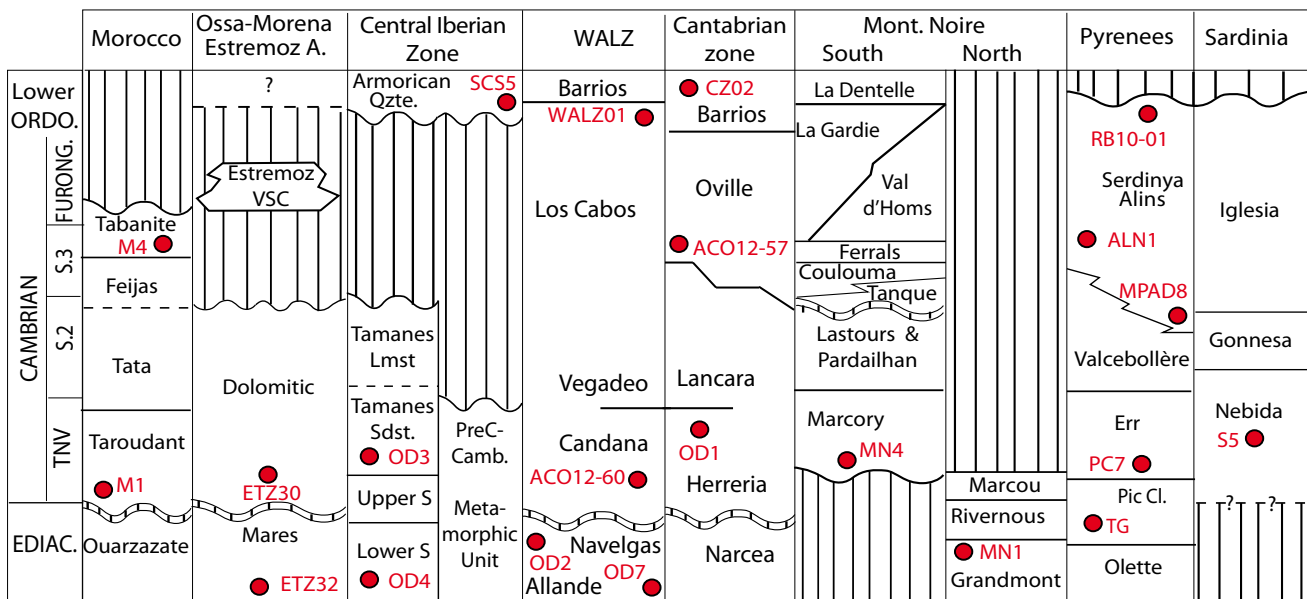


FIGURE 3. Schematic Ediacaran–Lower Ordovician stratigraphic chart showing setting of samples reported in this study: Avigad *et al.* (2012: samples M1 and M4, Anti-Atlas, Morocco and sample S5, SW Sardinia, Italy), Pereira *et al.* (2012: ETZ30 and ETZ32, Ossa-Morena Zone, Spain); Fernández-Suárez *et al.* (2014: OD3 and OD4, Central-Iberian Zone; OD2 and OD7, West Asturian-Leonese Zone; OD1, Cantabrian Zone, Spain); Shaw *et al.* (2014: SCS5, Central Iberian Zone; WALZ01, West Asturian-Leonese Zone; CZ02, Cantabrian Zone, Spain); Henderson *et al.* (2016: ACO12-57 and ACO12-60, Cantabrian Zone, Spain); Casas *et al.* (2015: TG0701, TG0702, TG0703 summarized under sample TG because of their sampling from a single lithostratigraphic unit, Spain); Padel *et al.* (2017: MN4, Montagne Noire, France (Figs. 6; 7). S= Series; Qtze.= Quartzite; VSC= volcanosedimentary complex; Estremoz A= Estremoz Anticline; Sdst.= Sandstone and Lmst.= limestone

MATERIAL AND METHODS

Three fine- to medium-grained sandstones were sampled in the Pyrenean Axial Zone for U-Pb detrital zircon geochronology: i) sample PC7 from a Terreneuvian Err metasandstone in the Puigmal Unit; ii) MPAD8 from a lowermost Serdinya metasandstone (encompassing the Cambrian Series 2–3 transition) in the Aspres Unit and iii) ALN1 from a Miaolingian Alins metasandstone in the central Pyrenees (Figs. 1; 2). Former U-Pb detrital zircon analyses were performed by Margalef *et al.* (2016) in sample RB-10-01, from a Lower Ordovician sandstone of the Seo Formation in the Rabassa Unit, central Pyrenees.

These four datasets are compared with previous analyses from Ediacaran to Ordovician detrital zircon grains following a SW-NE transect along the northwestern Gondwana margin (Fig. 3). The sample selection was based on i) distinct chronostratigraphic controls, ii) representative amounts of zircon grains to be statically acceptable for comparison and iii) precise sample location within the regional tectonostratigraphic units. The compilation includes over 50 samples but, based on the three discerning criteria stated above, only 19 samples were selected. These include case studies from the Moroccan Anti-Atlas (Avigad *et al.*, 2012: samples M1 and M4), the Ossa-Morena Zone (Pereira *et al.*, 2012: ETZ30 and ETZ32), the Central Iberian Zone (Fernández-Suárez *et al.*, 2014: OD3

and OD4; Shaw *et al.*, 2014: SCS5), the West Asturian-Leonese Zone (Fernández-Suárez *et al.*, 2014: OD2 and OD7; Shaw *et al.*, 2014: WALZ01), the Cantabrian Zone (Fernández-Suárez *et al.*, 2014: OD1; Shaw *et al.*, 2014: CZ02; Henderson *et al.*, 2016: ACO12-57 and ACO12-60), the Montagne Noire (Padel *et al.*, 2017a: MN4, MN1), the eastern Pyrenees (Casas *et al.*, 2015: TG0701, TG0702 and TG0703, named below sample TG because the three sandstones were sampled in the same structural and lithostratigraphic unit), and southern Sardinia (Avigad *et al.*, 2012: S5) (Fig. 3). Assignment of these samples to potential sedimentary sources follow the nomenclature reported by Avigad *et al.* (2003, 2012), Linnemann *et al.* (2011), Drost *et al.* (2011) and Pereira *et al.* (2012).

U-Pb analytical method

The zircon grains yielded by the new Pyrenean samples (PC7, MPAD8 and ALN1) were randomly hand-picked under a binocular microscope after grinding of fresh rocks followed by heavy liquid and magnetic separation. They were included in epoxy resin and then polished in order to expose their inner parts. Internal growth textures and morphologies of zircon grains were revealed using cathodoluminescence and back-scattered electron imaging under Scanning Electron Microscope (SEM) at the Laboratoire Océanologie et Géoscience of the University of Lille 1.

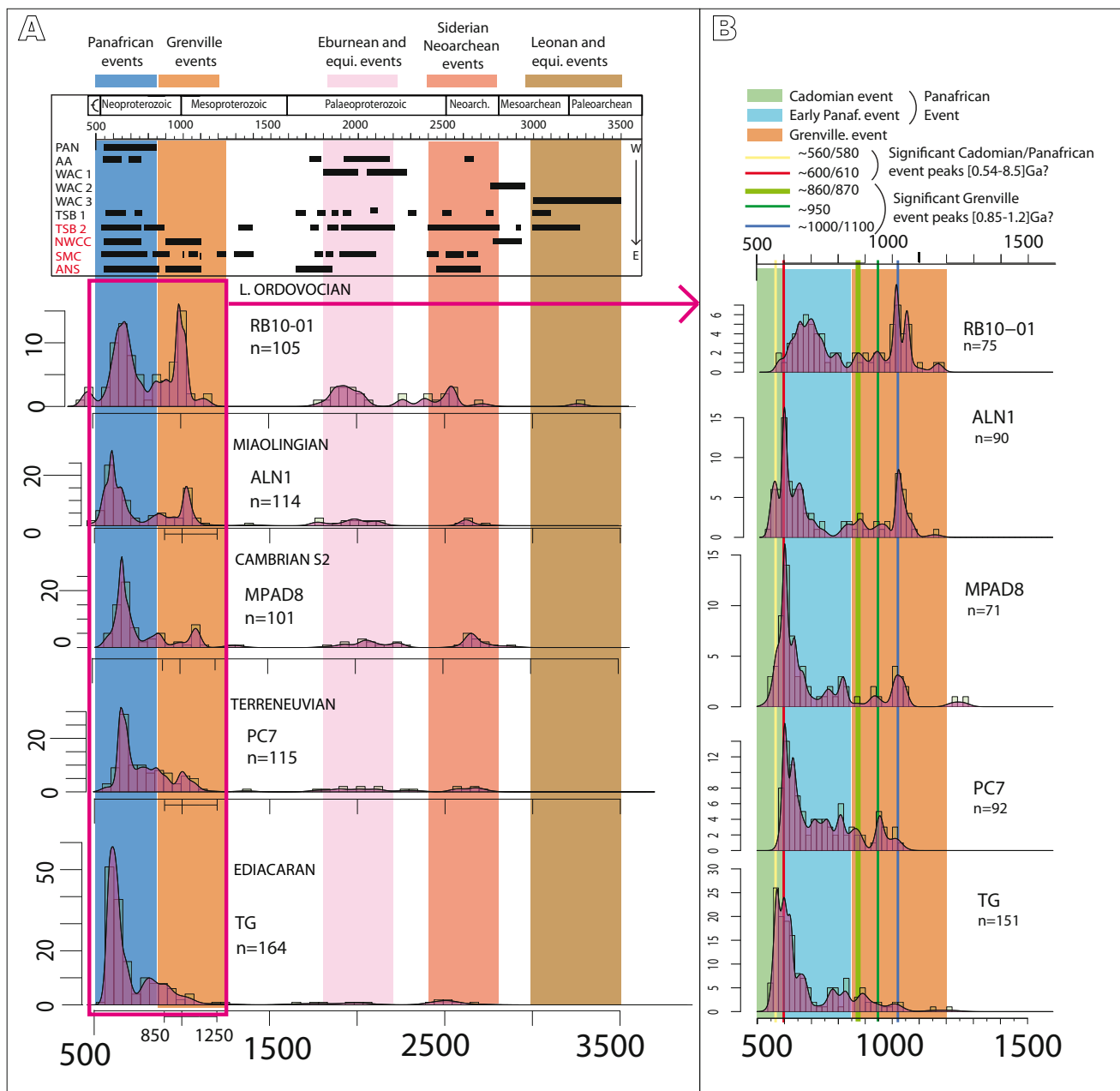


FIGURE 4. A) KDE plot for Ediacaran to Lower Ordovician samples from the Pyrenees. The upper part of the diagram shows potential 3500–500Ma zircon sources of detrital zircon populations and potential geological events linked to them. Sources are identified according to the methodology reported by Avigad *et al.* (2003, 2012), Drost *et al.* (2011), Linnemann *et al.* (2011) and Pereira *et al.* (2012). PAN= Panafrican and Cadomian event sources; AA= Anti-Atlasian event sources; WAC1= Eburnean event sources of the West African craton; WAC2= Liberian event sources of the West African craton; WAC3= Leonan event sources of the West African craton; TSB1= Trans-Saharan belt, Benin-Nigerian shield sources; TSB2= Trans-Saharan belt, Tuareg shield sources; SMC= Saharan metacraton; sources ANS= Arabian-Nubian shield sources; NWCC= Northwestern edge of Congo Craton sources. B) KDE plot for zircon populations included in the 1200-450Ma interval illustrating the evolution of some specific peaks through different samples; equo.: equivalent.

U-Pb *in situ* analysis of single grains were determined at the GeOHeLiS analytical platform (University of Rennes 1) by Laser Ablation Coupled with Plasma source Mass Spectrometry (LA-ICP-MS), using ablation spot diameters of $25\mu\text{m}$, energy pulse of 7J/cm^2 and repetition rates of 5Hz. Data were corrected for U-Pb

fractionation and for the mass bias by standard bracketing with repeated measurements of the GJ-1 zircon (Jackson *et al.*, 2004). Repeated analyses of the Plešovice zircon standard (Sláma *et al.*, 2008) treated as unknowns were used to control the reproducibility and accuracy of the corrections and yielded a concordia age of $336.7 \pm 0.8\text{Ma}$

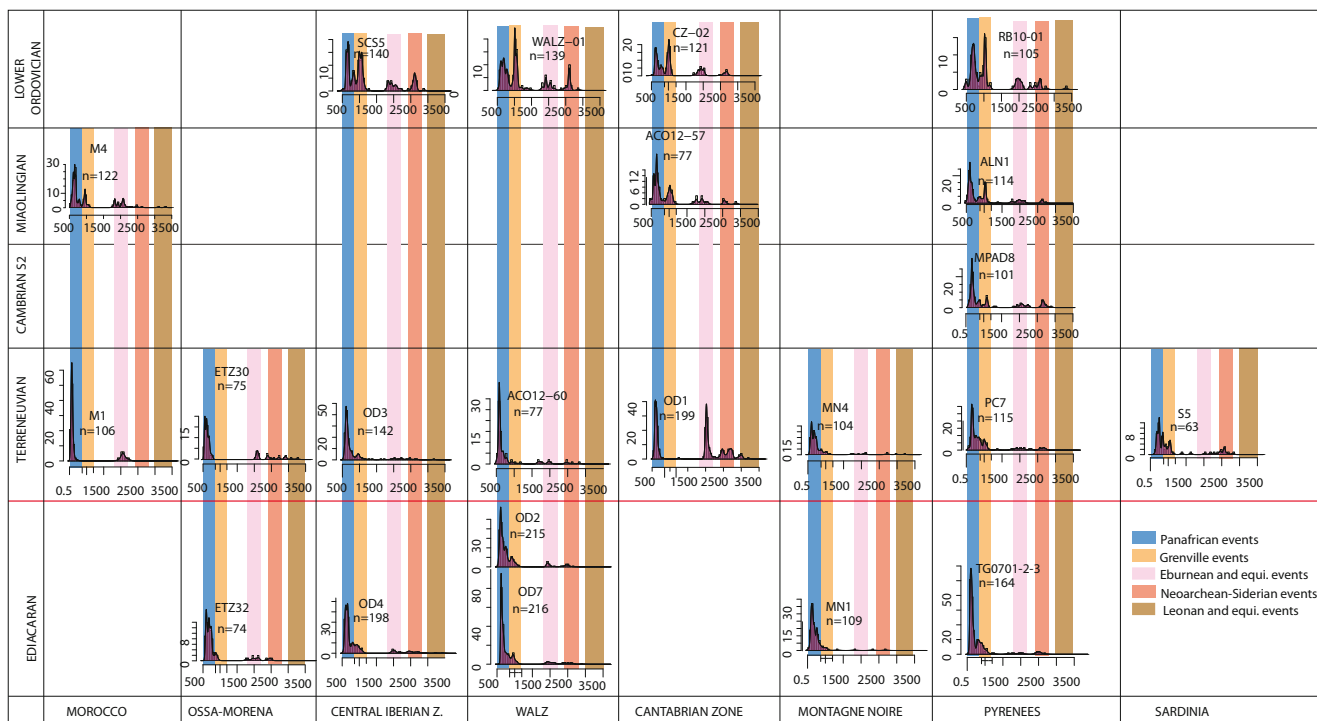


FIGURE 5. Comparison of Kernel Density Estimate plot for all samples included in this study.

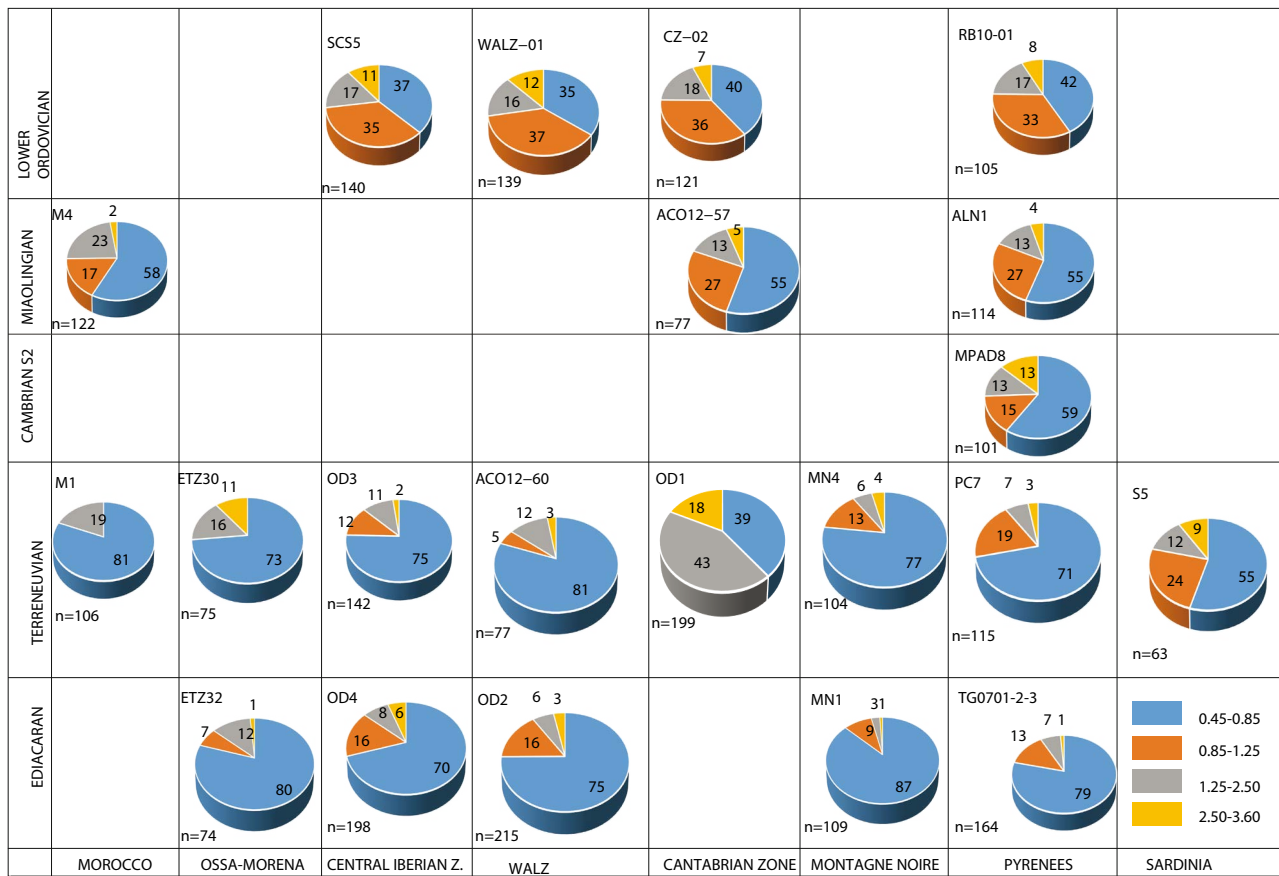


FIGURE 6. Pie chart with relative proportion of the different age groups identified in all the samples included in this study.

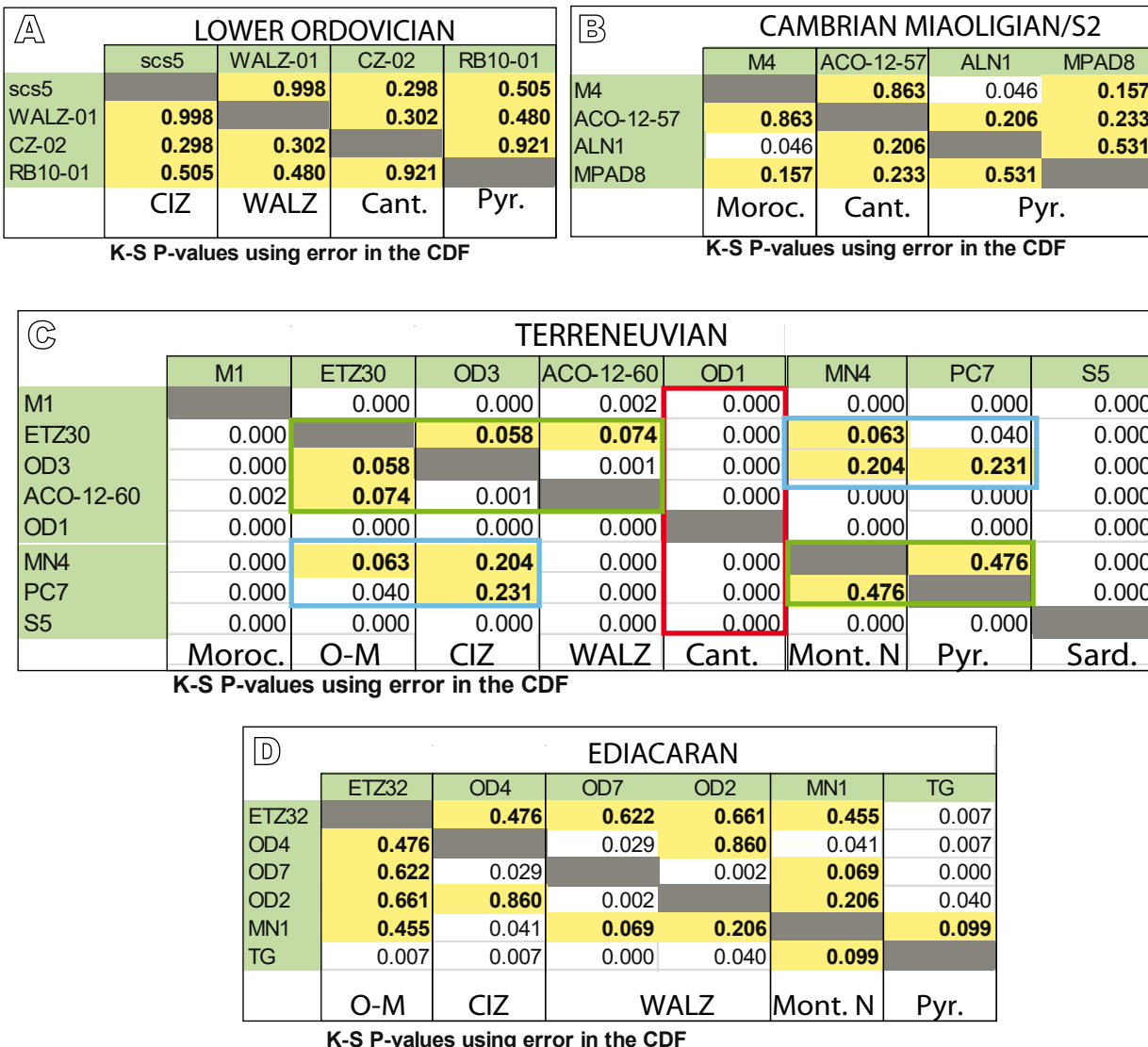


FIGURE 7. Results of K-S test displayed by all samples. Yellow boxes identify samples with probable identical parent zircon populations with a 95% confidence level. This test has been applied for samples of equivalent age: A) Lower Ordovician, B) Cambrian Miaolingian Series 2, C) Terreneuvian and D) Ediacaran. CIZ= Central Iberian Zone; WALZ= West Asturian-Leonese Zone; Cant= Cantabrian Zone; Pyr= Pyrenees; Moroc= Morocco; O-M= Ossa-Morena; Mont. N= Montagne Noire; Sard= Sardinia.

(n= 36; MSWD= 0.33). Data reduction was carried out with the GLITTER software (Van Achterbergh *et al.*, 2001). More information about the analytical protocol can be found in Manzotti *et al.* (2015), Padel *et al.* (2017a) and in Appendix I.

U-Pb data treatment: comparison of sources and tectonic settings

All data sets are summarized in Appendix II-IV, where the isotopic ratios and single apparent ages are reported with 1σ errors. In total, 115 grains were analysed from sample PC7, 107 from MPAD8, and 120 from ALN1. In this study, data treatment was made with the analyses

that were more than 90% concordant using the $^{207}\text{Pb}/^{206}\text{Pb}$ apparent ages for zircon older than 1000Ma, and the $^{206}\text{Pb}/^{238}\text{U}$ apparent ages for the grains that are younger than 1000Ma (Faure and Mensing, 2005; Meinholt *et al.*, 2011; Talavera *et al.*, 2012). The maximum depositional age is calculated using the age of the youngest zircon population from a cluster of at least three concordant analyses from three different grains overlapping in age at 2s (standard deviation), as proposed by Dickinson and Gehrels (2009), to ensure a statistically robust estimate of the maximum depositional ages. As suggested by Manzotti *et al.* (2015), KDE plots (Figs. 4; 5) were built using IsoplotR (Vermeesch, 2018) for sample comparisons with a specific focus on five geological

events: the Panafrican, Grenville, Eburnean (or related), Siderian–Neoarchean and Leonan (or related) events. Helped by this graphical proxy, a statistical comparison for equivalent cluster age proportion was made on Neoarchean–Siderian [3.6–2.5Ga], Siderian–Stenian [2.50–1.25Ga], Stenian–Tonian [1.25–0.85Ga] and Tonian–Ediacaran [0.85–0.45Ga] (Fig. 6).

A K-S test was applied to determine if contemporaneous siliciclastic sediments were supplied from similar sources (revealed by a spike on the age distribution) along the NW Gondwana margin (Fig. 7). The K-S test is a non-parametric probabilistic test, useful to compare age distributions from different samples and to discriminate potential statistical differences between them (Guynn and Gehrels, 2010). The test compares the cumulative probability curves, or cumulative distribution functions (CDF), of different zircon populations to evaluate the probability (P) that they might be different (Guynn and Gehrels, 2010). For a K-S test with a 95% confidence level, as used herein, a P-value lower than 0.05 means that the compared populations are significantly different.

Sedimentary basins can be distinguished according to their lithospheric basement, their position with respect to plate boundaries (intracratonic vs. plate margin), and their background plate motion (convergent, collisional, divergent or transform; Allen and Allen, 2005). Cawood et al. (2012) introduced a methodology to decipher the type of basin and their relative tectonic settings based on detrital zircon analysis; the authors provided a comparative CA-DA diagram, where the Cumulative Distribution Function (CDF) of zircon age is illustrated based on differences between Crystallization Ages (CA) and Depositional Ages (DA) of the detrital zircon grains. This empirical model considers that convergent settings induce large proportions of detrital zircon crystals with narrow unimodal KDE curves, linked to early magmatic arcs close, in space and time, to the depositional basin (*e.g.* fore-arc, back-arc, intra-arc and foreland cordillera basins). On the contrary, collisional, extensional and intracratonic settings (passive margin, rift and foreland basins) would induce a relatively delayed incorporation of detrital grains characterized by multimodal age distributions (compared to their crystallization age) through possible polyphase reworking. As a result, extensional tectonic settings can be deduced from detrital zircon analyses if CA-DA>150Ma at 5% of the CDF (step1). If step 1 is not reached, a CA-DA<100Ma at 30 % of CDF points to a convergent tectonic setting (magmatic arc-related basin; step 2). CA-DA diagrams for Cambrian–Early Ordovician times are used below to analyse variations in sediment sources along Northwest Gondwana. The applicability of this method to decipher the tectonic evolution of the margin is further discussed.

RESULTS: NEW DATA FROM THE PYRENEAN SAMPLES

In sample PC7 from the Err Formation (Fig. 4), 105 of the 115 analyses are at least 90% concordant. As the depositional age of this sample is Terreneuvian, an age of ~530Ma is selected for the CA-DA diagram (Fig. 9). PC7 displays a predominant Tonian–Cambrian [0.85–0.50Ga] group representing 71% of the data with a second major Stenian–Tonian [1.25–0.85Ga] group around 19% of the grains (Figs. 4; 6), a Siderian–Stenian [2.50–1.25Ga] group (7% of the data), and finally a Palaeoarchean–Neoarchean [3.6–2.5Ga] group representing 3% of the zircon grains. The three youngest concordant and overlapping analysis give a concordant maximum depositional age at 601.9 ± 3.3 Ma, MSWD= 1.8 (Appendix V).

In sample MPAD8 from the Serdinya Formation (Fig. 4), 103 of 107 analyses are 90% concordant or more. The depositional age of this sample is dated close to the Cambrian Epoch 2–Miaolingian boundary. Consequently an age of ~514Ma is selected for the CA-DA diagram transition (Fig. 9). In this sample, 59% of the detrital zircons belong to the Tonian–Cambrian [0.85–0.50Ga], 15% are part of a Stenian–Tonian [1.25–0.85Ga] group, while the Siderian–Stenian [2.50–1.25Ga] and Palaeoarchean–Neoarchean [3.6–2.5Ga] groups represent both 13% of the population (Figs. 4; 6). The three youngest concordant and overlapping analysis give a concordant maximum depositional age at 570.2 ± 3.0 Ma, MSWD= 0.019 (Appendix V).

In sample ALN1 from the Alins/Seo Formation (Fig. 4), 114 of the 120 analyses were at least 90% concordant. The age of this sample is Miaolingian hence an age of ~514Ma is selected for the CA-DA diagram (Fig. 9). In this sample, 55% of the detrital zircons belong to the upper Tonian–Cambrian [0.85–0.50Ga] group, 27 are part of the Stenian–Tonian [1.25–0.85Ga] group, 13% of the Siderian–Stenian [2.50–1.25Ga] group, and 4% of the Palaeoarchean–Neoarchean [3.6–2.5Ga] group (Figs. 4; 6). The three youngest concordant and overlapping analysis give a concordant maximum depositional age at 562.2 ± 3.1 Ma, MSWD= 0.57 (Appendix V).

Based on the late Ediacaran to Early Ordovician evolution of the detrital zircon populations from the Pyrenees, a progressive shift from Panafrican-dominant to more diverse sources, including older cratons, can be envisaged. Among these older sources, those related to Grenville events increase from 13% in Ediacaran sedimentary rocks to more than 30% in Ordovician sandstones (Fig. 6), reaching percentages comparable to the Panafrican sources (42%). Two peaks (610–600 and 580–560Ma) are predominant in the Panafrican sources, being the latter peak (580–560Ma) representative of regional Cadomian events (Fig. 4), such

as those recorded in the Pic de la Clape ignimbrites (Padel et al., 2018). The 580–560 Ma age peak ranges from almost dominant in the Ediacaran samples (TG) to nonexistent in the Terreneuvian ones, before their reappearance in Cambrian Epoch 2–Miaolingian samples.

These two peaks disappear in the Early Ordovician samples (Fig. 4), where they are replaced by sources revealing other early Panafrican events. The Grenville sources show two age peaks, which remain stable throughout the Ediacaran to Lower Ordovician samples, where the 1.1–1.0 Ga peak progressively increases until becoming the most important of all the Proterozoic sources (Fig. 4). As a result, the oldest sources, poorly represented in Ediacaran samples, progressively become more important as controlled by younger depositional ages arguing for sedimentary input from larger areas, probably involving more open and interconnected basins.

DISCUSSION

SW-NE trends in Terreneuvian sedimentary sources

The K-S tests (Fig. 7) characterize the evolution of Ediacaran to Early Ordovician provenance sources along the northwestern Gondwana margin. During the Ediacaran, two ends can be identified: i) a southwesternmost edge where Ossa-Morena shares its zircon pattern with the remaining Iberian Massif, and ii) a northeasternmost edge where the Pyrenees mainly shares its zircon pattern with the Montagne Noire.

During the Terreneuvian, the K-S test shows a possible palaeogeographic constraint with a SW edge (Anti-Atlas), a NE edge (Sardinia), and an intermediate domain (Cantabrian Zone) separating two transects: i) the southwestern Ossa-Morena, Central Iberian and West Asturian-Leonese Zones and ii) the northeastern Montagne Noire and Pyrenees domains (Fig. 7). As a consequence, after comparing zircon populations following a SW-NE-trend, a southwestern source can be recognized mainly feeding the Atlas–Ossa-Morena Rift, a northeastern source feeding the Sardinian margin, and an intermediate area, comprising the Pyrenees, the Montagne Noire and the remaining zones of the Iberian Massif. The effect of the Cantabrian Zone can be explained by a relation between a proximal to distal polarity with other Iberian zones. However, this configuration could also be linked to the presence of a palaeogeographic indentor (Fig. 10) equivalent to the Gondwana promontory model proposed by Dias et al. (2016).

Several characteristic Archaean–Palaeoproterozoic zircon populations are identified in all the Terreneuvian–Cambrian Epoch 2 samples. Even if they only represent

between 10 to 27% of the global analysed grains, there is a noticeable variation of their relative proportion along NW Gondwana, despite the lack of a distinct pattern probably due to the reduced number of zircon grains. A West African Craton source has often been mentioned to explain the presence of Archaean to Palaeoproterozoic zircon populations in the “lower Cambrian” successions (Avigad et al., 2012 for Morocco and Sardinia; Pereira et al., 2012 for Ossa-Morena Zone; Fernández-Suárez et al., 2014 for the central and northern Iberian Massif zones; Padel et al., 2017 for Montagne Noire). However, the influence of other sources (such as the Arabian Nubian Shield, Saharan Metacraton and Trans-Saharan Belt) cannot be ruled out for most of the studied areas. Although absent in the Terreneuvian–Cambrian Epoch 2 Moroccan sample, Neoarchaean zircon populations (which cannot originate from the West African Craton) are more abundant in other contemporaneous samples. This potentially demonstrates the influence of the Arabian Nubian Shield, the Saharan Metacraton and the Trans-Saharan Belt in the northeastern transect of NW Gondwana. Based on the results yielded by these Terreneuvian–Cambrian Series 2 samples, the Cantabrian Zone seemingly represents an exception with more than 60% of the analysed zircon grains derived from Archaean–Palaeoproterozoic sources. In addition, a significant peak around 2.5 Ga and the important influence of Meso- and Mesoarchean sources suggest that the Cantabrian Zone could reflect a central source, such as that of the Trans-Saharan Belt (TSB).

The Amazonian craton has been considered as another potential source for some Palaeo- and Mesoproterozoic zircon crystals sampled in NW Gondwana, or even as the single source for all of them (Fernández-Suárez et al., 2000; Linnemann et al., 2014). The involvement of Amazonian sources was proposed because there were no other ca. 1 Ga old sources known in the region at that time (Fernández-Suárez et al., 2014). Since then, such 1 Ga old sources have been identified from the Arabian Nubian shield, the Saharan Metacraton, the Trans-Saharan belt (Avigad et al., 2012; Be’eri-Shlevin et al., 2012) and, more recently, from the northwestern edge of the Congo Craton in Cameroun (Bernard et al., 2021). In accordance with Fernández-Suárez et al. (2014), the absence of 1.6–1.2 Ga zircon grains in different margins of NW Gondwana can be used as an argument to discard significant sources from the Amazonian craton. Therefore, this craton is not reported in Figures 4 and 10; we consider its influence to be, at best, minimal.

Terreneuvian–Cambrian Series 2 sediments from the Atlas–Ossa-Morena Rift are characterized by a predominant cluster of ca. 0.63–0.54 Ga grains, which represent between 81 and 73% of the analyzed zircon populations (Figs. 5; 6). Avigad et al. (2012) proposed a major contribution

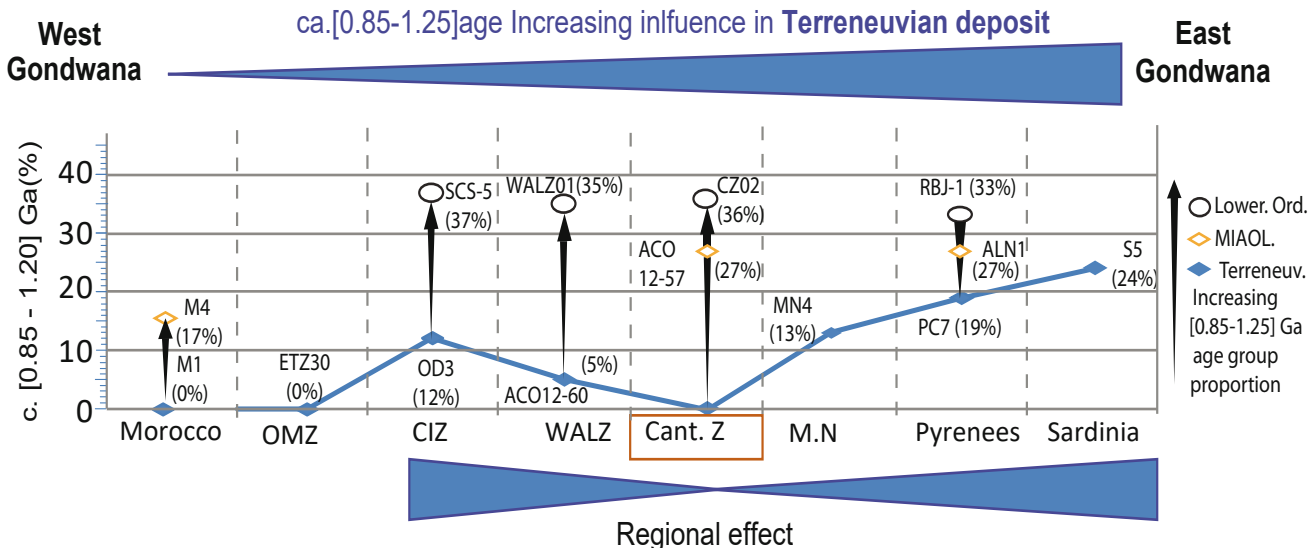


FIGURE 8. W-E transect of the northwestern Gondwana margin showing an increasing influence of Stenian–Tonian sources from the Saharan Metacraton and the Arabian-Nubian Shield in Cambro-Ordovician sediments; OMZ= Ossa-Morena Zone; CIZ= Central Iberian Zone; WALZ= West Asturian-Leonese Zone; Cant. Z= Cantabrian Zone; M.N= Montagne Noire

from the upper Ediacaran volcanic event represented by the Ouarzazate Supergroup (the so-called Ediacaran Anti-Atlasian Chain of Pouclet *et al.*, 2008) emplaced during the last stages of the Panafrican orogeny (Álvaro *et al.*, 2014b), and referred below to as the Anti-Atlasian source. Although Pereira *et al.* (2012) suggested that the 0.7–0.54Ga zircon grains from Ossa-Morena (ETZ30) could be derived from the Cadomian arc, the Anti-Atlasian (Blein *et al.*, 2014a, b) and/or TSB sources seem to fit better with the observed ca. 0.63–0.54 age group identified both in the Anti-Atlas and the Ossa-Morena Zone, where older Panafrican zircon crystals (0.95–0.65Ga) are absent or poorly represented. In the two intermediate areas (the Central Iberian and West Asturian-Leonese Zones vs. the Montagne Noire and the Pyrenees), separated by the Cantabrian Zone, 81 to 71% of the analyzed zircon grains form a 0.9–0.5Ga age group (Fig. 6), whereas they represent only 39% in the Cantabrian Zone. For this Panafrican sources, either western (Anti-Atlasian), central (Transsaharan Belt), or eastern (Arabian-Nubian Shield and Saharan Metacraton) sources may be invoked.

Zircon grains related to a 1.25–0.85Ga group (*i.e.* coeval to the Grenville orogeny elsewhere; Figs. 5; 6; 8) are generally associated with the Arabian-Nubian Shield, which was exhumed during Panafrican orogenic events (Caby, 2003; Liégeois *et al.*, 2003; Kroner and Stern, 2005), and/or with the Saharan Metacraton (Avigad *et al.*, 2003; Fernández-Suárez *et al.*, 2014; Shaw *et al.*, 2014; Padel *et al.*, 2017a, b), however, they should also be linked to the northwestern edge of the Congo Craton (Bernard *et al.*, 2021). Such an age group is absent in the “lower Cambrian” siliciclastic strata of the Anti-Atlas and the Ossa-Morena

Zone and shows a distinct progressive increase in percentage from the central to the northern Iberian zones (11%) to Sardinia (22%) (Figs. 5; 6; 8). Fernández-Suárez *et al.* (2014) further noticed that sample OD3 (Central Iberian Zone) revealed a zircon age distribution similar to that from “lower Cambrian” samples reported from the northwestern part of the Arabian-Nubian Shield (Israel and Jordan). The influence of both the eastern Arabian-Nubian Shield and the Saharan metacraton increases northeastward along NW Gondwana, where a possible influence of the northwestern edge of the Congo Craton should be also envisaged (Fig. 10).

Cambrian source evolution and related tectonic settings

Studies of detrital zircon grains yielded by Cambrian Series 2–Lower Ordovician sandstones of Northwest Gondwana are scarce. Only eight samples are available, including four from Cambrian Series 2-Miaolingian and four from Lower Ordovician strata (Figs. 5; 6). Chronological trends in provenance sources are tentatively interpreted based on K-S tests and CA-DA diagrams. According to K-S tests, there are no significant differences between zircon populations (Fig. 7). This supports a relative homogenization of provenance sources along Northwest Gondwana between Cambrian Epoch 2 to Early Ordovician times. The best age group to illustrate this homogenization is the Stenian–Tonian group (Fig. 8), whose proportion, as observed in the Pyrenees, increases from Ediacaran to Lower Ordovician sandstones. The Stenian–Tonian group, associated with sources from the Arabian Nubian Shield, the Saharan Metacraton and the northwestern edge of

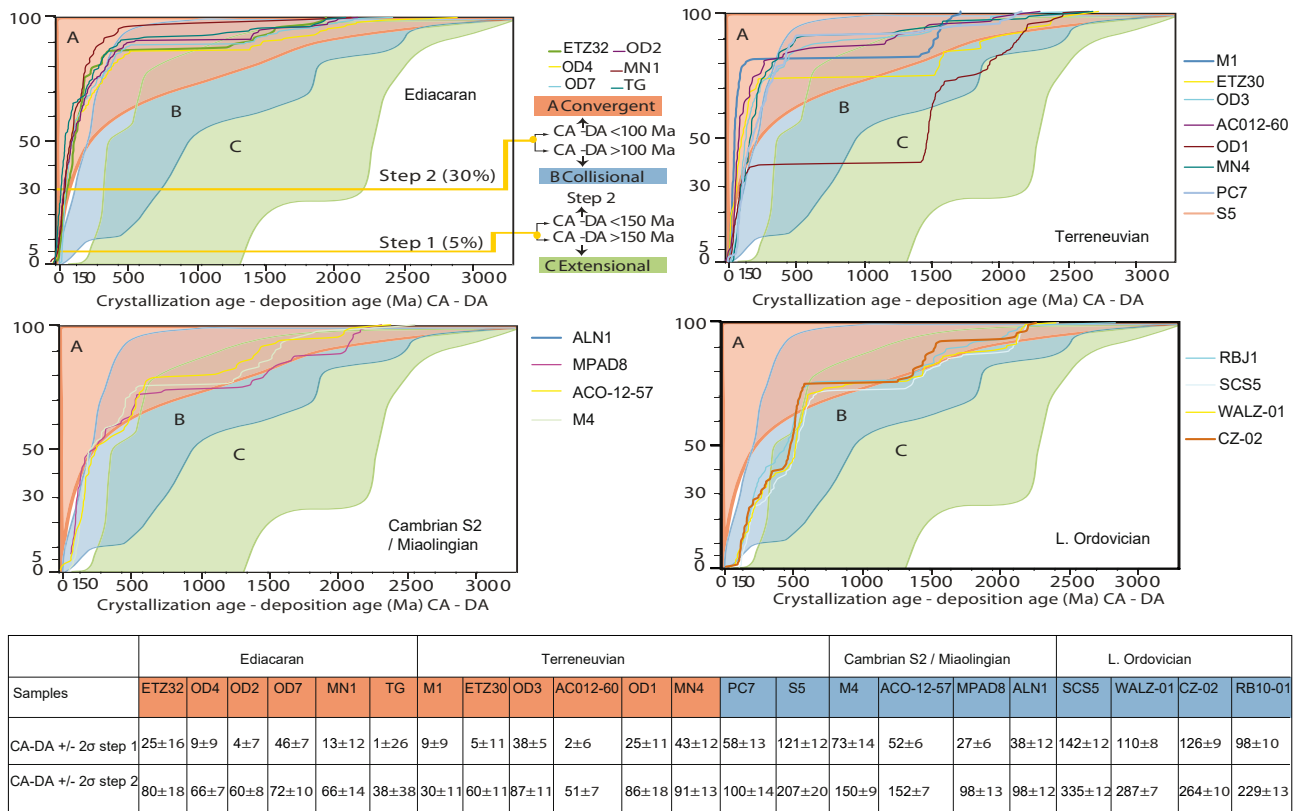


FIGURE 9. CA-DA diagrams illustrating the interpreted tectonic settings for the reported Terreneuvian–Lower Ordovician samples from Northwestern Gondwana; The table shows the numerical results at the 2 step of the test: an extensional tectonic setting can be deduced from detrital zircon analyses if CA-DA> 150Ma at 5% of the CDF (step1). If step 1 is not reached, a CA-DA< 100Ma at 30% of the CDF points to a convergent tectonic setting (magmatic arc-related basin; step 2), otherwise it could be interpreted as collisional tectonic setting. For abbreviations of samples, see text.

the Congo Craton, which did not influence the Atlas-Ossa-Morena Rift during the Terreneuvian, subsequently provided up to 16% of the inherited grains during the Miaolingian (Fig. 8). A comparison of isotopic Hf values in the Stenian-age population of zircons from Morocco and Sardinia, Avigad *et al.* (2012) suggested two distinct Stenian sources feeding the western and eastern edges of NW Gondwana. Figure 8 illustrates the evolution of this specific age group. During Terreneuvian times, the 1.25–0.85Ga age group suggests that the Pyrenees would be located between Montagne Noire and Sardinia. In the Cantabrian Zone, the 1.25–0.85Ga age group is not well-represented in the zircon population of sample OD1 (Fig. 8). In addition, the K/S test shows that OD1 appears to be significantly different from other Terreneuvian samples of the intermediate zone. These results suggest that, during the Terreneuvian, the Cantabrian margin was distinctive enough to represent the hinge of the southwestern and a northeastern transects. The evolution of this age group during the Ediacaran–Terreneuvian interval displays two distinct behaviours: the western Ossa-Morena and West Asturian-Leonese Zones transect is characterized by a lower proportion of the 1.25–0.85Ga group, whereas this age group is characterized by a progressive increase in the

eastern Montagne Noire and Pyrenees transect (Figs. 5; 6; 8). Although the early Palaeozoic palaeogeographic position of the Pyrenean margin cannot be definitely assessed, the analysis of this 1.25–0.85Ga age group suggests a strong affinity with the Montagne Noire and Sardinia, probably standing between them (Álvaro *et al.*, 2021).

At the end of Terreneuvian times, the above-reported SW-NE trend is interpreted to reflect a delayed shift in tectonic activity. The amalgamation of the Gondwana supercontinent (Stern, 1994; Ballèvre *et al.*, 2001; Meert, 2003; Kroner and Stern, 2005; Stampfli and von Raumer, 2008; Murphy *et al.*, 2013; Stampfli *et al.*, 2013; Linnemann *et al.*, 2014; Blein *et al.*, 2014a, b) is recorded in the studied area by the Panafrican and Cadomian orogens, which ended up close to the Ediacaran–Cambrian time interval. During the early Palaeozoic, the geodynamic setting of Northwest Gondwana changed drastically from convergent to extensional, marking the beginning of an interconnected rifting phase that ended with the opening of the Rheic Ocean (Ballèvre *et al.*, 2001; Linnemann *et al.*, 2007, 2008; Pereira *et al.* 2012; Stampfli *et al.*, 2013; Pouclet *et al.*, 2017).

Terreneuvian

Potential source (Ga)		
PAN	ANS	TSB
0.55-0.85	0.55-0.65	0.55-0.85
NWCC 0.55-0.85	0.9-1.1 1.65-1.85	0.85-1.4 1.65-2.2
0.9-1.1 2.7-2.9	2.45-2.7 3-3.25	2.4-2.8
SMC 0.55-0.8	WAC 0.85-1.6 1.75-2.1	2.75-2.95 3-3.5

- Possible sources input
 → Stenian-Tonian sources input
 1: Anti-Atlas
 2: Ossa-Morena
 3: Central Iberian Zone

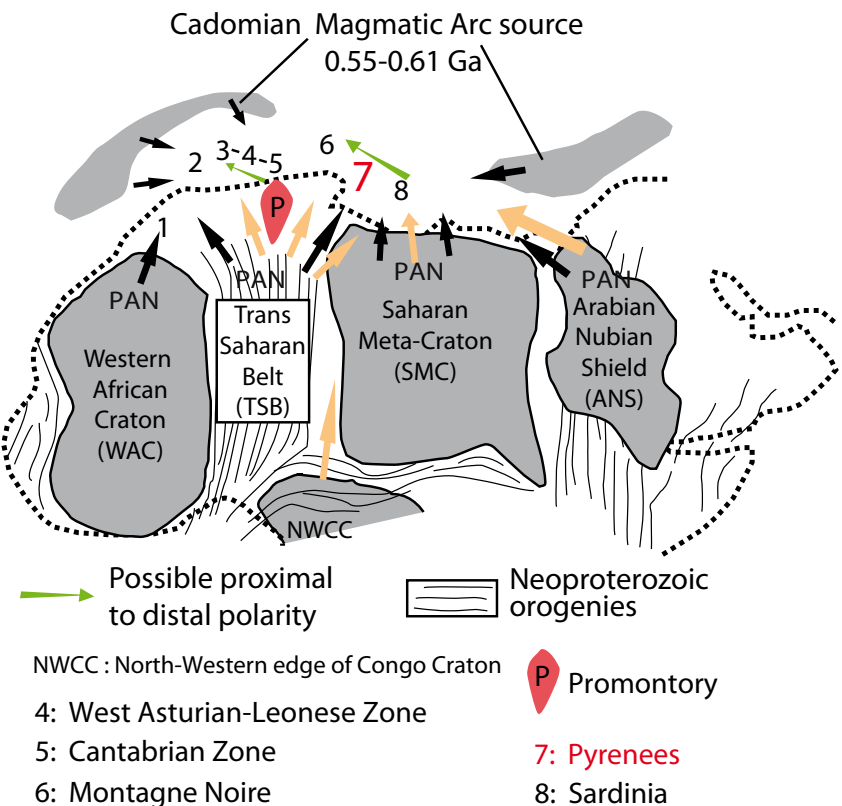


FIGURE 10. Tentative palaeoposition reconstruction of the different peri-Gondwana transects reported in the text according to the influence of their zircon supply potential sources. The promontory (P in the figure) is proposed as an effect of the Cantabrian Zone which be link to the presence of an indentation equivalent to the Gondwana promontory proposed, among others, by [Dias et al. \(2016\)](#).

The arc/rift/drift evolution is not clearly reflected by the CA-DA diagram (Fig. 9). Data from the Ediacaran samples fit well with a convergent setting. The Terreneuvian sandstones from the Anti-Atlas (M1), Ossa-Morena (ETZ30), Central Iberian (OD3), West Asturian-Leonese (ACo12-60), Cantabrian (OD1) Zones and the Montagne Noire (MN4) plot in the CA-DA diagram within the convergent field (A field in Fig. 9), while the remaining samples plot within the collisional field (B field in Fig. 9). These results disagree with other geological evidences, which rather support an extensional regime with the onset of rifting conditions along the margin ([Linnemann et al., 2007, 2008; Stampfli and von Raumer, 2008; Álvaro et al., 2016, 2021; Pouquet et al., 2017](#)). However, this apparent mismatch between the CA-DA model and the geological evidence can be linked to two major factors that controlled the zircon populations deposited in an early extensional setting, which are not integrated in the CA-DA model: i) the time-laps since the last convergent setting (as illustrated, for example, by [Cawood et al., 2012](#) for Furongian deposits from Avalonia) and ii) the distance between the sources and the setting of deposition. The effects on the CA-DA diagram, known as the “closeness of a recent source”, and its interpretation are well illustrated in the studied “lower Cambrian” samples.

The fast post-Panafrican and post-Cadomian shift from convergent to extensional conditions, and the short distances between the settings of deposition and the major Ediacaran Panafrican and Anti-Atlasian sources, explain their permanent influence in Terreneuvian sediments of the Atlas (M1)-Ossa-Morena (ETZ30) Rift, as illustrated by the major peak in zircon age distributions and the reduced CA-DA values. The influence of these sources subsequently vanished, resulting in a more flattened and equilibrated age distribution, with a more balanced influence of relatively distant sources of various ages, and higher CA-DA values. In our case study, the easternmost edge (Pyrenees and Sardinia) is rather distant from any source inherited from the late Meso- to Neoproterozoic orogens, such as the Panafrican or Anti-Atlasian ones (located to the Southwest), or the Arabian-Nubian Shield and Sahara metacraton (to the Northeast). Hence the Pyrenees and Sardinia display a more balanced distribution of zircon composition, increasing their relative CA-DA values, which could explain their “apparent” misleading position in the collisional field. From Cambrian Epoch 2 to Miaolingian times, the effect of the closeness to recent sources progressively decreased. In the present case, the different major Meso- to Neoproterozoic sources tend to enlarge their target to more distant basins, again stretching the zircon age curve

repartition and increasing the CA-DA value in siliciclastic successions (M4, ACO12-57, MPAD8, ALN1). Only the Lower Ordovician sandstones of the Central-Iberian Zone (SCS5, within error), deposited in “post-transitional” extensional settings (Shaw *et al.*, 2014; Margalef *et al.*, 2016; Pouclet *et al.*, 2017) and reflect a CA-DA particularity significative (CA-DA at step 1= 142 ± 12 Ma; Fig. 9).

Nonetheless, both the KDE and CA-DA diagrams for Terreneuvian successions suggest an eastward decreasing influence of the Panafrican and/or Anti-Atlasian sources, together with an increase in the influence of the Meso- to Neoproterozoic Arabian-Nubian Shield and Sahara sources, in a context of relatively rapid transition from convergent to extensional settings. The KDE and CA-DA diagrams also suggest a rapid change in geodynamic conditions from a Terreneuvian post-collisional phase, evolving to extensive dynamics that stabilised in the Furongian–Early Ordovician. The end of rifting conditions or rift-drift turnover led to the establishment of a passive margin that also affected the Occitan and South Armorican domains during early Ordovician times (Pouclet *et al.*, 2017).

Additional biogeographic links and distinct magmatic episodes support the palaeogeographic interpretations based on zircon population sources. The patch-reefs sampled in the Terrades inlier of the eastern Pyrenees have recently provided a rich fossil record comprising archaeocyathids, bradoriids, brachiopods, molluscs, tommotiids, chancelloriids, hyoliths and problematic microfossils (Perejón *et al.*, 1994; Wallet *et al.*, 2021), with strong biogeographic links with both the Montagne Noire and Sardinia. The Pyrenees also share with the Montagne Noire and Sardinia: i) the presence of late Ediacaran–early Terreneuvian felsic explosive calc-alkaline tuffs related to the Cadomian orogen, despite the absence of Cadomian metamorphic events (Álvaro *et al.*, 2014a; Padel *et al.*, 2017a, b, 2018); ii) a carbonate production across the Cambrian Series 2-Miaolingian transition; iii) the lack of the Furongian–Early Ordovician Toledanian Phase, associated with the onset of a break-up unconformity; and iv) a distinct record of the Mid–Ordovician Sardic Phase reflecting thermal doming, generalized denudation of areas uplifted under subaerial conditions, and intrusion of massive peraluminous granitic bodies (Álvaro *et al.*, 2016, 2021). All these complementary observations suggest that the Cambrian Pyrenean margin was probably located between the Cantabrian-Montagne Noire and the Sardinian margins of West Gondwana (Figs. 8; 10).

CONCLUSIONS

Detrital zircon grains from Ediacaran–Lower Ordovician sandstones and quartzites sampled in the Pyrenees were

dated by LA-ICPMS in order to assess their provenance sources. The resulting age distributions are compared to other available datasets from neighbouring margins, such as Morocco, the Iberian Peninsula, France and Sardinia. K-S test, KDE and CA-DA diagrams were used to compare zircon populations estimating their possible correlation with the arc/rift/drift geodynamic evolution recorded in Northwest Gondwana.

During Terreneuvian times, three areas can be distinguished: a southwestern edge (comprising the Atlas-Ossa-Morena Rift), a central transitional area (encompassing the central and northern Iberian Massif Zones, the Montagne Noire and the Pyrenees), and a northeastern edge (Sardinia). The relative influence of major sediment sources follows a SW–NE trend. Indeed, the Panafrican-Anti-Atlasian sources predominate within the southwesternmost successions, whereas the influence of the Arabian-Nubian Shield and Sahara Metacraton sources increases northeastward. The Terreneuvian trend gradually disappeared throughout Cambrian Epoch 2 to Early Ordovician times. This pattern reflects the evolution of geodynamic settings along NW Gondwana, with a rapid post-Panafrican shift to rifting and drifting conditions. Although the palaeogeographic position of the Pyrenean margin cannot be definitely assessed, the analysis of zircon populations from Cambro-Ordovician strata supports former biogeographic, stratigraphic and magmatic studies, suggesting a strong affinity with the Montagne Noire and Sardinia domains, tentatively locating the Pyrenees between both margin transects.

ACKNOWLEDGMENTS

This research was founded by the RGF program of the French Geological Survey (BRGM). This paper is a contribution to project CGL2013-48877-P from Spanish MINECO. François Guillot, Olivier Blein, Cecilio Quesada and Cesar Witt are warmly thanked for stimulating discussions about Cadomian geodynamics. The authors appreciate revisions by Noel Moreira (Evora, Portugal) and an anonymous reviewer.

REFERENCES

- Allen, P.A., Allen, J.R., 2005. Basin Analysis. Principles and Applications. Cambridge, Blackwell Scientific Publications, 562pp.
- Altumi, M.M., Elicki, O., Linnemann, U., Hofmann, M., Sagawe, A., Gärtner, A., 2013. U-Pb LA-ICP-MS detrital zircon ages from the Cambrian of Al Qarqaf Arch, central-western Libya: provenance of the West Gondwanan sand sea at the dawn of the early Palaeozoic. Journal of African Earth Sciences, 79, 74–97.

- Álvaro, J.J., Bauluz, B., Clausen, S., Devaere, L., Imaz, A.G., Monceret, E., Vizcaíno, D., 2014a. Stratigraphy of the Cambrian–Lower Ordovician volcanosedimentary complexes in the northern Montagne Noire, France. *Stratigraphy*, 11, 83–96.
- Álvaro, J.J., Benziane, F., Thomas, R., Walsh, G.J., Yazidi, A., 2014b. Neoproterozoic–Cambrian stratigraphic framework of the Anti-Atlas and the Ouzzellagh promontory (High Atlas), Morocco. *Journal of African Earth Sciences*, 98, 1–15.
- Álvaro, J.J., Colmenar, J., Monceret, E., Pouclet, A., Vizcaíno, D., 2016. Late Ordovician (post-Sardic) rifting branches in the North Gondwanan Montagne Noire and Mounhoumet massifs of southern France. *Tectonophysics*, 681, 111–123.
- Álvaro, J.J., Sánchez-García, T., Puddu, C., Casas, J.M., Díez-Montes, A., Liesa, M., Oggiano, G., 2020. Comparative geochemical study on Furongian–earliest Ordovician (Toledanian) and Ordovician (Sardic) felsic magmatic events in south-western Europe: underplating of hot mafic magmas linked to the opening of the Rheic Ocean. *Solid Earth*, 11, 2377–2409.
- Álvaro, J.J., Casas, J.M., Quesada, C., 2021. Reconstructing the pre-Variscan puzzle of Cambro–Ordovician basement rocks in the southwestern European margin of Gondwana. In: Murphy, J.B., Strachan, R.A., Quesada, C. (eds.). *Pannotia to Pangaea: Neoproterozoic and Paleozoic Orogenic Cycles in the Circum-Atlantic Region*. Geological Society, London, Special Publications 503, 531–562.
- Avigad, D., Kolodner, K., McWilliams, M., Persing, H., Weissbroad, T., 2003. Origin of northern Gondwana Cambrian sandstone revealed by detrital zircon SHRIMP. *Geology*, 31, 227–230.
- Avigad, D., Gerde, A., Morag, N., Bechstädt, T., 2012. Coupled U-Pb-Hf of detrital zircons of Cambrian sandstones from Morocco and Sardinia: implications for provenance and Precambrian crustal evolution of North Africa. *Gondwana Research*, 21, 690–703.
- Avigad, D., Rossi, Ph., Gerdes, A., Abdo, A., 2018. Cadomian metasediments and Ordovician sandstone from Corsica: detrital zircon U-Pb-Hf constrains on their provenance and paleogeography. *International Journal of Earth Sciences*, 107, 2803–2818.
- Ballèvre, M., Le Goff, E., Hébert, R., 2001. The tectonothermal evolution of the Cadomian belt of northern Britany, France: a Neoproterozoic volcanic arc. *Tectonophysics*, 331, 19–43.
- Ballèvre, M., Bosse, V., Ducassou, C., Pitra, P., 2009. Palaeozoic history of the Armorican Massif: models for the tectonic evolution of the suture zones. *Comptes Rendus Geoscience*, 341, 174–201.
- Ballouard, C., Poujol, M., Zeh, A., 2018. Multiple crust reworking in the French Armorican Variscan belt: implication for the genesis of uranium-fertile leucogranites. *International Journal of Earth Sciences*, 107, 2317–2336.
- Barnolas, A., Chiron, J.C., 1996. Synthèse géologique et géophysique des Pyrénées. Tome 1: Cycle hercynien. Orléans-Madrid, Bureau de Recherche Géologique et Minière – Instituto Tecnológico y Geominero de España, 729pp.
- Be'eri-Shlevin, Y., Eyal, M., Eyal, Y., Whitehouse, M.J., Livinovsky, B., 2012. The Sa'al volcano-sedimentary complex (Sinai, Egypt): a latest Mesoproterozoic volcanic arc in the northern Arabian Nubian Shield. *Geology*, 40, 403–406.
- Bernard, J., Couëffé, R., Blein, O., Vic, G., Buscail, F., Tchokona Seuwui, D., Wongolo Djombol, M.H., Tucker, R., Cagnard, F., Duron, J., Martelet, G., Bailly, L., Chevillard, M., Colin, S., Chabot, L., Gutierrez, T., Lahaye, Y., Anaba Fotze, Q.M., Eno-Tabi Lobe Makia, G., Ndapeh Ndellejeng, B., Essomba, Y.H., 2021. Carte géologique du Cameroun à 1/200 000 – Feuilles Batouri (NB-33-III), Betare-Oya (NB-33-IX), Meiganga (NB-33-XV), Belel (NB-33-XXI), Rey-Bouba (NC-33-III). Ministère des Mines, de l'Industrie et du Développement technologique du Cameroun, Yaoundé, Notice explicative, 224pp.
- Blein, O., Baudin, T., Soulaimani, A., Cocherie, A., Chèvremont, P., Admou, H., Ouainaimi, H., Hafid, A., Razin, P., Bouabdelli, M., Roger, J., 2014a. New geochemical, geochronological and structural constraints on the Ediacaran evolution of the south Sirwa, Agadir-Melloul and Iguerda inliers, Anti-Atlas, Morocco. *Journal of African Earth Sciences*, 98, 47–71.
- Blein, O., Baudin, T., Chèvremont, Ph., Soulaimani, A., Admou, H., Gasquet, D., Cocherie, A., Egal, E., Youbi, N., Razin, Ph., Bouabdelli, M., Gombert, Ph., 2014b. Geochronological constraints on the polycyclic magmatism in the Bou Azzer-El Graara inlier (Anti-Atlas, Morocco). *Journal of African Earth Sciences*, 99, 287–306.
- Caby, R., 2003. Terrane assembly and geodynamic evolution of central-western Hoggar: a synthesis. *Journal of African Earth Sciences*, 37, 133–159.
- Casas, J.M., Murphy, J.B., 2018. Unfolding the arc: the use of pre-orogenic constraints to assess the evolution of the Variscan belt in Western Europe. *Tectonophysics*, 736, 47–61.
- Cass, J.M., Palacios, T., 2012. First biostratigraphical constraints on the pre–Upper Ordovician sequences of the Pyrenees based on organic-walled microfossils. *Comptes Rendus Geoscience*, 344, 50–56.
- Casas, J.M., Castañeiras, P., Navidad, M., Liesa, M., Carreras, J., 2010. New insights into the Late Ordovician magmatism in the Eastern Pyrenees: U-Pb SHRIMP zircon data from the Canigó massif. *Gondwana Research*, 17, 317–324.
- Casas, J.M., Navidad, M., Castañeiras, P., Liesa, M., Aguilar, C., Carreras, J., Hofman, M., Gärtner, A., Linnemann, U., 2015. The Late Neoproterozoic magmatism in the Ediacaran series of the Eastern Pyrenees: new ages and isotope geochemistry. *International Journal of Earth Sciences*, 104, 909–925.
- Castañeiras, P., Navidad, M., Liesa, M., Carreras, J., Casas, J.M., 2008. U-Pb zircon ages (SHRIMP) for Cadomian and Lower Ordovician magmatism in the Eastern Pyrenees: new insights in the pre-Variscan evolution of the northern Gondwana margin. *Tectonophysics*, 46, 228–239.
- Cawood, P.A., Hawkesworth, C.J., Dhuime, B., 2012. Detrital zircon record and tectonic setting. *Geology*, 40, 875–878.
- Cochelin, B., Lemire, B., Denèle, Y., De Saint Blanquat, M., Lahfid, A., Duchêne, S., 2018. Structural inheritance in the

- Central Pyrenees: the Variscan to Alpine tectonometamorphic evolution of the Axial Zone. *Journal of the Geological Society*, 175, 336–351.
- Cocherie, A., Baudin, T., Autran, A., Guerrot, C., Fanning, M., Laumonier, B., 2005. U-Pb zircon (ID-TIMS and SHRIMP) evidence for the early Ordovician intrusion of metagranites in the late Proterozoic Canaveilles Group of the Pyrenees and the Montagne Noire (France). *Bulletin de la Société géologique de France*, 176, 269–282.
- Couzinié, S., Laurent, O., Chelle-michou, C., Bouilhol, P., Paquette, J.L., Gannoun, A.M., Moyen, J.F., 2019. Detrital zircon U-Pb-Hf systematics of Ediacaran metasediments from the French Massif Central: consequences for the crustal evolution of the north Gondwana margin. *Precambrian Research*, 324, 269–284.
- Deloule, E., Alexandrov, P., Cheillett, A., Laumonier, B., Barbey, P., 2002. In situ U-Pb zircon ages for Early Ordovician magmatism in the eastern Pyrenees, France: the Canigou orthogneisses. *International Journal of Earth Sciences*, 91, 398–405.
- Denèle Denèle, Y., Barbey, P., Deloule, E., Pelleter, E., Olivier, Ph., Gleizes, G., 2009. Middle Ordovician U-Pb age of the Aston and Hospitalet orthogneissic laccoliths: their role in the Variscan evolution of the Pyrenees. *Bulletin de la Société géologique de France*, 180(3), 209–216.
- Dias, R., Ribeiro, A., Romão, J., Coke, C., Moreira, N., 2016. A review of the arcuate structures in the Iberian Variscides; constraints and genetic models. *Tectonophysics*, 681, 170–194.
- Dickinson, W.R., Gehrels, G.E., 2009. Use of U-Pb ages of detrital zircons to infer maximum depositional ages of strata: a test against a Colorado Plateau Mesozoic database. *Earth and Planetary Science Letters*, 288, 115–125.
- Drost, K., Gerdes, A., Jeffries, T., Linnemann, U., Storey, C., 2011. Provenance of Neoproterozoic and early Paleozoic siliciclastic rocks of the Tepla-Barrandian unit (Bohemian Massif): evidence from U-Pb detrital zircon ages. *Gondwana Research*, 19, 213–231.
- Faure, G., Mensing, T.M., 2005. Isotopes: principles and applications. Wiley, Hoboken, 928pp.
- Fernández-Suárez, J., Gutiérrez-Alonso, G., Jenner, G.A., Tubrett, M.N., 2000. New ideas on the Proterozoic–Early Palaeozoic evolution of NW Iberia: insights from U-Pb detrital zircon ages. *Precambrian Research*, 102, 185–206.
- Fernández-Suárez, J., Gutiérrez-Alonso, G., Pastor-Galán, D., Hofmann, M., Murphy, J.B., Linnemann, U., 2014. The Ediacaran–Early Cambrian detrital zircon record of NW Iberia: possible sources and paleogeographic constraints. *International Journal of Earth Sciences*, 103, 1335–1357.
- Gehrels, G., 2014. Detrital zircon U-Pb geochronology applied to tectonics. *Annual Review of Earth and Planetary Sciences*, 42, 127–149.
- Gutiérrez-Alonso, G., Fernández-Suarez, J., Jeffries, T.E., Jenner, G.A., Tubrett, M.N., Cox, R., Jackson, S.E., 2003. Terrane accretion and dispersal in the northern Gondwana margin. An Early Paleozoic analogue of a long-lived active margin. *Tectonophysics*, 365, 221–232.
- Gutiérrez-Alonso, G., Fernández-Suarez, J., Pastor-Galán, D., Johnston, S.T., Linnemann, U., Hofmann, M., Shaw, J., Colmenero, J.R., Hernández, P., 2015. Significance of detrital zircons in Siluro–Devonian rocks from Iberia. *Journal of the Geological Society*, 172, 309–322.
- Guynn, J., Gehrels, G., 2010. Comparison of detrital zircon age distributions using the K-S test. Last accessed: April 2010 Website: <https://sites.google.com/a/laserchron.org/laserchron/>
- Henderson, B.J., Collins, W.J., Murphy, J.B., Gutiérrez-Alonso, G., Hand, M., 2016. Gondwanan basement terranes of the Variscan–Appalachian orogeny: Baltican, Saharan and West African hafnium isotopes fingerprints in Avalonia, Iberia and the Armorican Terranes. *Tectonophysics*, 681, 278–304.
- Jackson, S.E., Pearson, N.J., Griffin, W.L., Belousova, E.A., 2004. The application of laser-ablation-inductively coupled plasma-mass spectrometry to in situ U-Pb zircon geochronology. *Chemical Geology*, 211, 47–69.
- Kroner, A., Stern, R.J., 2005. Pan-African orogeny. *Encyclopedia of Geology*, 1, 1–12.
- Kydonakis, K., Kostopoulos, D., Poujol, M., Brun, J.P., Papanikolaou, D., Paquette, J.L., 2014. The dispersal of the Gondwana super-fan system in the eastern Mediterranean: new insights from detrital zircon geochronology. *Gondwana Research*, 25, 1230–1241.
- Laumonier, B., Abad, A., Alonso, J.L., Baudelot, S., Bessière, G., Besson, M., Bouquet, C., Bourrouilh, R., Brula, P., Carreras, J., Centène, A., Courjault-Radé, R., Courtessole, R., Fauconnier, D., García-Sansegundo, J., Guitard, G., Moreno-Eiris, E., Perejón, A., Vizcaíno, D., 1996. Cambro–Ordovicien. In: Barnolas, A., Chiron, J.C. (eds.). *Synthèse géologique et géophysique des Pyrénées. Tome 1: Cycle hercynien*. Orléans–Madrid, Bureau de Recherche Géologique et Minière – Instituto Tecnológico y Geominero de España, 729pp.
- Laumonier, B., Autran, A., Barbey, P., Cheillett, A., Baudin, T., Cocherie, A., Guerrot, C., 2004. Conséquences de l'absence de socle cadomien sur l'âge et la signification des séries pré-varisques (anté-Ordovicien supérieur) du sud de la France (Pyrénées, Montagne Noire). *Bulletin de la Société géologique de France*, 175, 105–117.
- Laumonier, B., Calvet, M., Wiazemsky, M., Barbey, P., Marignac, C., Lambert, J., Lenoble, J.L., 2015. Notice explicative de la Carte géologique de la France (1/50.000), feuille Céret (1096). Bureau de Recherche Géologique et Minière, Orléans.
- Lemire, B., Cochelin, B., Duchene, S., de Saint Blanquat, M., Poujol, M., 2019. Origin and duration of late orogenic magmatism in the foreland of the Variscan belt (Lesponne - Chiroulet - Neouvielle area, French Pyrenees). *Lithos*, 336, 183–201.
- Liégeois, J.P., Latouche, L., Boughara, M., Navez, J., Guiraud, M., 2003. The LATEA metacraton (Central Hoggar, Tuareg Shield, Algeria): behaviour of an old passive margin during the Pan-African orogeny. *Journal of African Earth Sciences*, 37, 161–190.

- Liesa, M., Carreras, J., Castiñeiras, P., Casas, J.M., Navidad, M., Vila, M., 2011. U-Pb zircon of Ordovician magmatism in the Albera Massif (Eastern Pyrenees). *Geologica Acta*, 9(1), 93–101.
- Linnemann, U., Gerdes, A., Drost, K., Buschmann, B., 2007. The continuum between Cadomian Orogenesis and opening of the Rheic Ocean: constraints from LA-ICP-MS U-Pb zircon dating and analysis of plate-tectonic setting (Saxo-Thuringian Zone, NE Bohemian massif, Germany). In: Linnemann, U., Nance, D., Kraft, P., Zulauf, G. (eds.). *The Evolution of the Rheic Ocean: from Avalonian–Cadomian Active Margin to Alleghenian–Variscan Collision*. Geological Society of America, 423 (Special Papers), 423, 61–96.
- Linnemann, U., Pereira, F., Jeffries, T.E., Drost, K., Gerdes, A., 2008. The Cadomian Orogeny and the opening of the Rheic Ocean: the diachrony of geotectonic processes constrained by LA-ICP-MS U-Pb zircon dating (Ossa-Morena and Saxo-Thuringian Zones, Iberian and Bohemian Massifs). *Tectonophysics*, 461, 21–43.
- Linnemann, U., Ouzegane, K., Draren, A., Hofmann, M., Becker, S., Gärtner, A., Sagawe, A., 2011. Sands of West Gondwana: an archive of secular magmatism and plate interactions – a case study from the Cambro–Ordovician section of the Tassili Ouan Ahaggar (Algerian Sahara) using U–Pb LA-ICP-MS detrital zircon ages. *Lithos*, 123, 188–203.
- Linnemann, U., Gerdes, A., Hofmann, M., Marko, L., 2014. The Cadomian Orogen: Neoproterozoic to Early Cambrian crustal growth and orogenic zoning along the periphery of the West African Craton – Constraints from U-Pb zircon ages and Hf isotopes (Schwarzburg Antiform, Germany). *Precambrian Research*, 244, 236–278.
- Manzotti, P., Poujol, M., Ballèvre, M., 2015. Detrital zircon in blueschist-facies metaconglomerates: implications for the Early Permian palaeo-topography of the Western Alps. *International Journal of Earth Sciences*, 104, 703–731.
- Margalef, A., Castiñeiras, P., Casas, J.M., Navidad, M., Montserrat, L., Linnemann, U., Hofmann, M., Gärtner, A., 2016. Detrital zircons from the Ordovician rocks of the Pyrenees: geochronological constraints and provenance. *Tectonophysics*, 681, 124–134.
- Martínez, E.J., Iriondo, A., Dietsch, C., Aleinikoff, J.N., Peucat, J.J., Cirès, J., Reche, J., Capdevila, R., 2011. U-Pb SHRIMP-RG zircon ages and Nd signature of lower Paleozoic rifting-related magmatism in the Variscan basement of the Eastern Pyrenees. *Lithos*, 127, 10–23.
- Martínez Catalán, J.R., Arenas, R., Díaz García, F., González Cuadra, P., Gómez-Barreiro, J., Abati, J., Castiñeiras, P., Fernández-Suárez, J., Sánchez Martínez, S., Andonaegui, P., González Clavijo, E., Díez Montes, A., Rubio Pascual, E.J., Valle Aguado, B., 2007. Space and time in the tectonic evolution of the northwestern Iberian Massif: implications for the Variscan belt. In: Hatcher, R.D.Jr., Carlson, M.P., McBride, J.H., Martínez Catalán, J.R. (eds.). *4-D Framework of Continental Crust*. Geological Society of America, 200 (Memoirs), 403–423.
- Meert, J.G., 2003. A synopsis of events related to the assembly of eastern Gondwana. *Tectonophysics*, 362, 1–40.
- Meinhold, G., Morton, A.C., Fanning, C.M., Frei, D., Howard, J.P., Phillips, R.J., Strogen, D., Whitham, A.G., 2011. Evidence from detrital zircons for recycling of Mesoproterozoic and Neoproterozoic crust recorded in Paleozoic and Mesozoic sandstones of southern Libya. *Earth and Planetary Science Letters*, 312, 164–175.
- Meinhold, G., Morton, A.C., Avigad, D., 2013. New insights into peri-Gondwana paleogeography and the Gondwana super-fan system from detrital zircon U-Pb ages. *Gondwana Research*, 23, 661–665.
- Mezger, J., Gerdes, A., 2016. Early Variscan (Visean) granites in the core of central Pyrenean gneiss domes: implications from laser ablation U-Pb and Th-Pb studies. *Gondwana Research*, 29, 181–198.
- Murphy, J.B., Keppie, J.D., Dostal, J., Nance, R.D., 1999. Neoproterozoic–early Paleozoic evolution of Avalonia. Geological Society of America, 336 (Special Papers), 253–266.
- Murphy, J.B., Pisarvesky, S.A., Nance, R.D., Keppie, J.D., 2004. Neoproterozoic–Early Paleozoic evolution of peri-Gondwana terranes: implications for Laurentia–Gondwana connections. *International Journal of Earth Sciences*, 93, 659–682.
- Murphy, J.B., Pisarvesky, S.A., Nance, R.D., 2013. Potential geodynamic relationships between the development of peripheral orogens along the northern margin of Gondwana and the amalgamation of West Gondwana. *Mineralogy and Petrology*, 107, 635–650.
- Nance, D.R., Murphy, J.B., Keppie, J.D., 2002. A Cordilleran model for the evolution of Avalonia. *Tectonophysics*, 352, 11–31.
- Nance, R.D., Murphy, J.B., Strachan, R.B., Keppie, J.D., Gutiérrez-Alonso, G., Fernández-Suárez, J., Quesada, C., Linnemann, U., D'lemos, R., Pisarvesky, S.A., 2008. Neoproterozoic–early Palaeozoic tectonostratigraphy and palaeogeography of the peri-Gondwanan terranes: Amazonian v. West African connections. In: Ennih, N., Liégeois, J.P. (eds.). *The Boundaries of the West African Craton*. London, The Geological Society, 297 (Special Publication), 345–383.
- Padel, M., Clausen, S., Álvaro, J.J., Casas, J.M., 2017a. Review of the Ediacaran–Lower Ordovician (pre–Sardic) stratigraphic framework of the Eastern Pyrenees, southwestern Europe. *Geologica Acta*, 16(4), 339–355.
- Padel, M., Álvaro, J.J., Clausen, S., Guillot, E., Poujol, M., Chichorro, M., Monceret, E., Pereira, M.F., Vizcaíno, D., 2017b. U-Pb laser ablation ICP-MS zircon dating across the Ediacaran–Cambrian transition of the Montagne Noire, southern France. *Comptes Rendus Geoscience*, 349, 380–390.
- Padel, M., Álvaro, J.J., Casas, J.M., Clausen, S., Poujol, M., Sánchez-García, T., 2018. Cadomian volcanosedimentary complexes across the Ediacaran–Cambrian transition of the Eastern Pyrenees, southwestern Europe. *International Journal of Earth Sciences*, 107, 1579–1601.
- Pastor-Galán, D., Gutiérrez-Alonso, G., Fernández-Suárez, J., Murphy, J.B., Nieto, E., 2013. Tectonic evolution of NW Iberia

- during the Paleozoic inferred from the geochemical record of detrital rocks in the Cantabrian Zone. *Lithos*, 182–183, 211–228.
- Pereira, M.F., Solá, A.R., Chichorro, M., Lope, L., Gerdes, A., Silva, J.B., 2012. North-Gondwana assembly, break-up and paleogeography: U-Pb isotope evidence from detrital and igneous zircons of Ediacaran and Cambrian rocks of SW Iberia. *Gondwana Research*, 22, 866–881.
- Perejón, A., Moreno-Eiris, E., Abad, A., 1994. Montículos de arqueociatos y calcimicrobios del Cámbrico inferior de Terrades, Gerona (Pirineo oriental, España). *Boletín de la Real Sociedad Española de Historia Natural (Sección Geológica)*, 89, 55–95.
- Pouclet, A., Álvaro, J.I., Bardintzeff, J.-M., Gil Imaz, A., Monceret, E., Vizcaíno, D., 2017. Cambrian–Early Ordovician volcanism across the South Armorican and Occitan Domains of the Variscan Belt in France: Continental break-up and rifting of the northern Gondwana margin. *Geosciences Frontiers*, 8, 25–64.
- Shaw, J., Gutiérrez-Alonso, G., Johnston, S.T., Galán, D.P., 2014. Provenance variability along the Early Ordovician north Gondwana margin: paleogeographic and tectonic implications of U-Pb detrital zircon ages from the Armorican Quartzite of the Iberian Variscan belt. *Geological Society of America Bulletin*, 26, 702–719.
- Sláma, J., Košler, J., Condon, D.J., Crowley, J.L., Gerdes, A., Hanchar, J.M., Horstwood, M.S.A., Morris, G.A., Nasdala, L., Norberg, N., Schaltegger, U., Schoene, B., Tubrett, M.N., Whitehouse, M.J., 2008. Plešovice zircon – a new natural reference material for U-Pb and Hf isotopic microanalysis. *Chemical Geology*, 249, 1–35.
- Stampfli, G.M., von Raumer, J., 2008. The birth of the Rheic ocean – Early Paleozoic subsidence patterns and subsequent tectonic plate scenarios. *Tectonophysics*, 461, 9–20.
- Stampfli, G.M., Hochard, C., Vérard, C., Wilhem, C., von Raumer, J., 2013. The formation of Pangea. *Tectonophysics*, 593, 1–19.
- Stern, R.J., 1994. Arc assembly and continental collision in the Neoproterozoic east African orogen: implication for the consolidation of Gondwana. *Annual Review of Earth and Planetary Sciences*, 22, 319–351.
- Talavera, C., Montero, P., Martínez Poyatos, D., Williams, I.S., 2012. Ediacaran to Lower Ordovician age for rocks ascribed to the Schist-Graywacke Complex (Iberian Massif, Spain): evidence from detrital zircon SHRIMP U-Pb geochronology. *Gondwana Research*, 22, 928–942.
- Van Achterbergh, E., Ryan, C.G., Jackson, S.E., Griffin, W.L., 2001. Data reduction software for LA-ICP-MS: appendix. In: Sylvester, P.J. (ed.). *Laser Ablation-ICP-mass spectrometry in the Earth Sciences: principles and applications*. Mineralogical Association of Canada, Short Courses Series, 29, 239–243.
- Vermeesch, P., 2018. IsoplotR: A free and open toolbox for geochronology. *Geoscience Frontiers*, 9, 1479–1493.
- Wallet, E., Padel, M., Devaere, L., Clausen, S., Álvaro, J.I., Laumonier, B., 2022. Cambrian Age 3 small shelly fossils from the Terrades inlier, southern Pyrenees, Spain: biostratigraphic and paleobiogeographic implications. *Journal of Paleontology*, 96, 552–582.

Manuscript received December 2021;
revision accepted July 2022;
published Online October 2022.

APPENDIX I

TABLE I.

ALN1	Pb (ppm)	U (ppm)	Th/U	Isotopic Ratios				rho	Apparent Ages				Conc. (%)		
				$^{207}\text{Pb}/^{235}\text{U}$	1sigAbsErr	$^{206}\text{Pb}/^{238}\text{U}$	1sigAbsErr		$^{207}\text{Pb}/^{206}\text{Pb}$	1sigAbsErr	$^{206}\text{Pb}/^{238}\text{U}$	1sigAbsErr			
ZR25	18	164	1.9	0.628	0.008	0.078	0.001	0.85	551	27	483	5	495	5	98
ZR15	38	408	1.0	0.651	0.008	0.079	0.001	0.92	586	24	492	5	509	5	97
ZR106	108	1283	0.2	0.700	0.008	0.085	0.001	0.93	583	24	529	6	539	5	98
ZR118	245	2767	0.4	0.694	0.008	0.086	0.001	0.94	555	24	531	6	535	5	99
ZR57	54	658	0.1	0.708	0.009	0.087	0.001	0.92	571	24	537	6	544	5	99
ZR97	45	480	0.6	0.730	0.009	0.088	0.001	0.92	618	24	542	6	557	5	97
ZR99	66	668	0.7	0.723	0.009	0.088	0.001	0.94	593	23	543	6	552	5	98
ZR96	18	199	0.5	0.768	0.010	0.088	0.001	0.84	722	27	543	6	579	6	94
ZR64	35	412	0.1	0.733	0.009	0.089	0.001	0.90	591	25	551	6	558	5	99
ZR7	15	147	0.9	0.741	0.010	0.089	0.001	0.88	612	26	551	6	563	6	98
ZR83	188	2275	0.0	0.731	0.009	0.090	0.001	0.95	575	23	553	6	557	5	99
ZR46	54	578	0.4	0.740	0.009	0.091	0.001	0.93	571	24	560	6	562	5	100
ZR37	15	173	0.2	0.736	0.009	0.091	0.001	0.91	559	25	561	6	560	5	100
ZR50	25	278	0.3	0.745	0.009	0.091	0.001	0.91	582	25	561	6	565	5	99
ZR59	30	299	0.7	0.742	0.009	0.091	0.001	0.91	569	25	562	6	564	5	100
ZR3	23	258	0.2	0.777	0.009	0.092	0.001	0.94	643	23	568	6	584	5	97
ZR117	12	103	1.1	0.787	0.011	0.093	0.001	0.84	657	27	572	6	590	6	97
ZR96	63	693	0.1	0.803	0.010	0.095	0.001	0.94	659	23	583	6	599	5	97
ZR16	16	165	0.4	0.772	0.010	0.095	0.001	0.89	570	25	584	6	581	6	100
ZR12	48	430	0.9	0.772	0.009	0.095	0.001	0.95	562	23	586	6	581	5	101
ZR58	67	578	1.1	0.803	0.010	0.095	0.001	0.93	644	24	587	6	598	5	98
ZR27	71	779	0.1	0.812	0.010	0.095	0.001	0.94	666	23	587	6	604	5	97
ZR104	18	207	0.0	0.814	0.012	0.096	0.001	0.78	665	30	589	6	605	7	97
ZR79	70	789	0.0	0.825	0.010	0.096	0.001	0.94	695	23	589	6	611	6	96
ZR111	196	2162	0.1	0.778	0.009	0.096	0.001	0.95	566	23	589	6	584	5	101
ZR28	6	56	0.9	0.779	0.012	0.096	0.001	0.72	567	33	590	7	585	7	101
ZR4	78	709	0.8	0.805	0.010	0.096	0.001	0.97	634	23	591	6	600	5	99
ZR92	23	244	0.2	0.833	0.011	0.096	0.001	0.89	703	25	592	6	615	6	96
ZR53	49	539	0.1	0.791	0.010	0.096	0.001	0.93	583	24	594	6	592	5	100
ZR103	165	1762	0.2	0.802	0.009	0.097	0.001	0.96	607	23	595	6	598	5	100
ZR38	46	512	0.1	0.814	0.010	0.097	0.001	0.95	637	23	596	6	605	5	99
ZR47	14	121	1.0	0.853	0.011	0.097	0.001	0.88	734	25	597	6	626	6	95
ZR49	63	654	0.2	0.859	0.011	0.098	0.001	0.87	734	25	601	7	630	6	95
ZR115	56	596	0.1	0.818	0.010	0.098	0.001	0.92	627	24	602	6	607	6	99
ZR61	30	230	1.5	0.830	0.010	0.099	0.001	0.91	636	24	607	7	613	6	99
ZR112	22	220	0.3	0.847	0.011	0.099	0.001	0.89	680	25	608	7	623	6	97
ZR19	33	298	0.7	0.833	0.010	0.099	0.001	0.93	637	24	609	7	615	6	99
ZR66	57	595	0.1	0.820	0.010	0.100	0.001	0.96	581	23	616	7	608	5	101
ZR39	36	355	0.3	0.848	0.010	0.101	0.001	0.94	646	23	617	7	624	6	99
ZR95	23	204	0.6	0.906	0.011	0.102	0.001	0.90	751	24	627	7	655	6	96
ZR114	33	319	0.3	0.917	0.012	0.103	0.001	0.89	771	25	629	7	661	6	95
ZR21	11	104	0.4	0.862	0.012	0.103	0.001	0.84	638	27	630	7	631	6	100
ZR69	14	120	0.8	0.871	0.012	0.103	0.001	0.86	658	26	630	7	636	6	99
ZR101	33	309	0.3	0.882	0.011	0.104	0.001	0.93	650	23	640	7	642	6	100
ZR85	32	292	0.6	0.914	0.012	0.104	0.001	0.88	726	25	640	7	659	6	97
ZR52	9	92	0.2	0.908	0.013	0.105	0.001	0.81	699	28	643	7	656	7	98
ZR34	13	108	0.8	0.921	0.012	0.105	0.001	0.85	728	26	644	7	663	7	97
ZR45	39	372	0.3	0.902	0.012	0.106	0.001	0.87	661	26	650	7	653	6	100
ZR26	19	155	0.8	0.915	0.012	0.107	0.001	0.88	682	25	653	7	660	6	99
ZR36	46	443	0.2	0.901	0.011	0.107	0.001	0.94	644	23	655	7	652	6	100
ZR88	20	172	0.6	0.944	0.012	0.107	0.001	0.88	736	25	657	7	675	6	97
ZR113	2	16	0.9	0.940	0.021	0.108	0.001	0.54	717	47	660	8	673	11	98
ZR43	29	191	1.8	0.938	0.011	0.109	0.001	0.93	692	24	666	7	672	6	99
ZR90	12	102	0.6	0.947	0.013	0.109	0.001	0.80	707	28	667	7	677	7	99
ZR80	30	254	0.5	0.958	0.012	0.112	0.001	0.92	678	24	684	7	682	6	100
ZR56	21	181	0.5	0.967	0.012	0.113	0.001	0.90	673	25	691	7	687	6	101
ZR35	18	138	1.0	1.003	0.013	0.114	0.001	0.90	733	25	697	7	705	6	99
ZR75	13	103	0.7	1.000	0.014	0.115	0.001	0.84	715	27	701	8	704	7	100
ZR33	20	166	0.2	1.094	0.013	0.120	0.001	0.91	809	23	731	8	750	7	97
ZR108	10	78	0.7	1.057	0.015	0.120	0.001	0.81	735	28	732	8	732	7	100
ZR89	4	28	0.6	1.262	0.021	0.133	0.002	0.72	894	32	805	9	829	9	97
ZR18	32	234	0.3	1.270	0.015	0.135	0.002	0.94	884	23	814	9	833	7	98
ZR110	41	280	0.5	1.276	0.016	0.137	0.002	0.92	855	23	828	9	835	7	99
ZR62	89	603	0.6	1.308	0.015	0.138	0.002	0.96	890	22	834	9	849	7	98
ZR68	44	304	0.3	1.350	0.016	0.141	0.002	0.96	906	22	853	9	868	7	98
ZR6	32	216	0.4	1.378	0.017	0.144	0.002	0.94	917	22	865	9	880	7	98
ZR54	175	1030	0.9	1.441	0.017	0.145	0.002	0.94	988	22	873	9	906	7	96
ZR84	61	413	0.3	1.410	0.017	0.145	0.002	0.93	944	23	873	9	893	7	98
ZR30	47	298	0.5	1.476	0.019	0.148	0.002	0.90	997	23	889	9	921	8	97
ZR77	28	180	0.4	1.450	0.018	0.152	0.002	0.93	911	23	910	10	910	7	100
ZR22	24	121	1.3	1.529	0.020	0.155	0.002	0.89	972	24	929	10	942	8	99
ZR2	22	138	0.5	1.545	0.019	0.157	0.002	0.93	968	22	940	10	948	8	98
ZR81	32	192	0.6	1.546	0.019	0.159	0.002	0.90	944	23	951	10	949	8	100
ZR78	61	406	0.0	1.591	0.019	0.162	0.002	0.95	965	22	968	10	967	7	100
ZR20	68	380	0.6	1.613	0.019	0.162	0.002	0.95	989	22	969	10	975	7	99
ZR73	28	204													

TABLE I. Continued

ALN1	Pb (ppm)	U (ppm)	Th/U	Isotopic Ratios					Apparent Ages					Conc.(%)	
				$^{207}\text{Pb}/^{235}\text{U}$	1sigAbsErr	$^{206}\text{Pb}/^{238}\text{U}$	1sigAbsErr	ρ	$^{207}\text{Pb}/^{206}\text{Pb}$	1sigAbsErr	$^{206}\text{Pb}/^{238}\text{U}$	1sigAbsErr	$^{207}\text{Pb}/^{235}\text{U}$	1sigAbsErr	
ZR76	34	209	0.2	1.642	0.020	0.164	0.002	0.93	1007	22	978	10	987	8	98
ZR94	68	382	0.7	1.589	0.019	0.158	0.002	0.94	1007	22	948	10	966	7	96
ZR63	22	112	1.1	1.631	0.020	0.162	0.002	0.90	1010	23	970	10	982	8	97
ZR74	16	63	2.2	1.698	0.023	0.169	0.002	0.85	1011	25	1006	11	1008	9	100
ZR70	16	82	0.7	1.708	0.024	0.170	0.002	0.83	1012	26	1012	11	1012	9	100
ZR87	31	173	0.5	1.680	0.021	0.170	0.002	0.91	975	23	1013	11	1001	8	103
ZR23	33	146	1.4	1.717	0.021	0.170	0.002	0.93	1021	22	1012	11	1015	8	99
ZR105	36	177	1.0	1.715	0.021	0.170	0.002	0.90	1021	23	1011	11	1014	8	99
ZR91	143	879	0.4	1.590	0.018	0.157	0.002	0.98	1027	21	940	10	966	7	94
ZR17	8	41	0.9	1.667	0.023	0.164	0.002	0.84	1029	25	981	10	996	9	97
ZR71	53	255	1.2	1.677	0.021	0.165	0.002	0.92	1030	23	986	10	1000	8	97
ZR32	30	156	1.0	1.648	0.020	0.162	0.002	0.93	1040	22	966	10	989	8	95
ZR40	14	75	0.7	1.733	0.022	0.170	0.002	0.89	1040	24	1012	11	1021	8	98
ZR41	21	117	0.5	1.791	0.022	0.174	0.002	0.93	1058	23	1035	11	1042	8	99
ZR5	47	255	0.9	1.652	0.020	0.161	0.002	0.94	1059	22	960	10	990	8	94
ZR1	20	98	1.0	1.803	0.022	0.175	0.002	0.94	1063	22	1039	11	1047	8	98
ZR65	122	778	0.5	1.513	0.018	0.146	0.002	0.96	1076	21	877	9	936	7	87
ZR98	109	592	0.2	2.002	0.023	0.186	0.002	0.97	1145	21	1102	11	1116	8	97
ZR100	8	77	0.2	1.113	0.018	0.096	0.001	0.72	1300	30	590	7	760	9	58
ZR60	12	41	1.2	2.835	0.037	0.233	0.003	0.87	1389	23	1350	14	1365	10	98
ZR67	201	823	0.5	3.177	0.037	0.217	0.002	0.98	1735	19	1266	13	1452	9	84
ZR9	54	142	1.1	4.593	0.054	0.310	0.004	0.96	1758	19	1740	17	1748	10	99
ZR107	62	230	0.2	3.918	0.046	0.264	0.003	0.96	1759	19	1511	15	1617	9	92
ZR93	105	367	0.2	4.253	0.049	0.281	0.003	0.97	1797	19	1595	16	1684	10	94
ZR14	16	48	0.6	4.820	0.061	0.304	0.004	0.91	1878	21	1713	17	1788	11	95
ZR109	59	198	0.1	4.841	0.057	0.299	0.003	0.95	1918	19	1686	17	1792	10	93
ZR42	117	324	0.6	5.318	0.062	0.323	0.004	0.97	1946	19	1806	18	1872	10	96
ZR82	116	360	0.8	4.571	0.055	0.276	0.003	0.94	1955	19	1574	16	1744	10	89
ZR10	111	283	1.0	5.397	0.063	0.324	0.004	0.98	1966	18	1811	18	1884	10	96
ZR11	39	85	1.6	5.659	0.069	0.338	0.004	0.94	1976	20	1879	19	1925	11	97
ZR13	21	51	0.6	6.206	0.074	0.365	0.004	0.95	2005	19	2006	20	2005	10	100
ZR24	36	103	0.5	5.381	0.065	0.316	0.004	0.94	2007	19	1771	18	1882	10	94
ZR102	208	582	0.4	5.783	0.067	0.328	0.004	0.97	2067	18	1831	18	1944	10	94
ZR51	186	441	0.6	6.691	0.079	0.374	0.004	0.96	2093	19	2050	20	2071	10	99
ZR116	56	141	0.5	6.462	0.078	0.359	0.004	0.93	2105	19	1978	19	2041	11	97
ZR48	183	458	0.4	6.776	0.079	0.371	0.004	0.96	2131	18	2034	20	2083	10	98
ZR31	69	109	1.3	11.235	0.130	0.469	0.005	0.97	2594	17	2480	23	2543	11	98
ZR44	534	1190	0.1	10.341	0.119	0.429	0.005	0.97	2604	17	2302	22	2466	11	95
ZR86	132	284	0.6	9.642	0.115	0.396	0.004	0.94	2621	18	2150	21	2401	11	92
ZR55	109	206	0.4	11.496	0.136	0.472	0.005	0.95	2623	18	2491	23	2564	11	98
ZR8	93	154	0.7	12.907	0.150	0.503	0.006	0.98	2708	17	2627	25	2673	11	99
ZR29	212	277	0.5	23.846	0.285	0.278	0.003	0.95	4562	16	1580	16	3262	12	72

TABLE II.

mpad8	Pb (ppm)	U (ppm)	Th/U	Isotopic Ratios					Apparent Ages						
				$^{207}\text{Pb}/^{235}\text{U}$	1sigAbsErr	$^{206}\text{Pb}/^{238}\text{U}$	1sigAbsErr	rho	$^{207}\text{Pb}/^{206}\text{Pb}$	1sigAbsErr	$^{206}\text{Pb}/^{238}\text{U}$	1sigAbsErr	$^{207}\text{Pb}/^{235}\text{U}$	1sigAbsErr	
ZR101	101	1035	0.9	0.666	0.008	0.0820	0.0009	0.91	565	25	508	5	518	5	98
ZR111	24	268	0.6	0.726	0.009	0.0834	0.0009	0.86	712	26	516	6	554	6	93
ZR46	36	386	0.6	0.708	0.009	0.0852	0.0009	0.87	612	26	527	6	543	5	97
ZR42	21	267	0.0	0.711	0.009	0.0856	0.0010	0.85	613	27	530	6	545	6	97
ZR36	84	874	0.7	0.754	0.009	0.0876	0.0010	0.94	690	23	541	6	571	5	95
ZR48	92	912	0.7	0.743	0.009	0.0901	0.0010	0.93	598	24	556	6	564	5	99
ZR4	23	191	1.3	0.764	0.011	0.0907	0.0010	0.81	642	28	560	6	576	6	97
ZR107	35	360	0.5	0.759	0.009	0.0920	0.0010	0.88	598	25	567	6	574	5	99
ZR108	29	327	0.2	0.752	0.009	0.0928	0.0010	0.88	560	26	572	6	569	6	100
ZR52	38	294	1.6	0.749	0.009	0.0928	0.0010	0.87	550	26	572	6	568	6	101
ZR7	23	199	1.1	0.782	0.011	0.0931	0.0011	0.82	639	28	574	6	587	6	98
ZR78	95	780	1.4	0.788	0.009	0.0942	0.0010	0.92	629	24	580	6	590	5	98
ZR28	158	1769	0.1	0.825	0.01	0.0946	0.0011	0.90	717	24	583	6	611	6	95
ZR47	39	355	0.7	0.809	0.01	0.0950	0.0011	0.91	667	24	585	6	602	6	97
ZR37	25	272	0.1	0.796	0.01	0.0958	0.0011	0.92	612	24	590	6	595	6	99
ZR95	122	1362	0.0	0.827	0.01	0.0963	0.0011	0.94	685	23	593	6	612	5	97
ZR24	29	216	1.3	0.888	0.012	0.0964	0.0011	0.84	832	26	593	6	645	7	92
ZR72	97	971	0.4	0.817	0.009	0.0968	0.0011	0.94	647	23	596	6	606	5	98
ZR54	26	214	1.0	0.815	0.011	0.0970	0.0011	0.85	639	27	597	6	605	6	99
ZR20	13	124	0.5	0.809	0.011	0.0975	0.0011	0.82	611	28	600	7	602	6	100
ZR25	22	199	0.7	0.955	0.013	0.0977	0.0011	0.84	956	26	601	7	681	7	88
ZR76	154	1400	0.7	0.83	0.01	0.0978	0.0011	0.93	660	23	601	6	614	5	98
ZR32	11	83	1.6	0.812	0.012	0.0979	0.0011	0.78	609	30	602	7	603	7	100
ZR45	19	161	0.9	0.817	0.011	0.0979	0.0011	0.85	622	26	602	6	607	6	99
ZR57	83	755	0.6	0.85	0.01	0.0980	0.0011	0.90	707	24	602	6	625	6	96
ZR59	29	267	0.6	0.845	0.011	0.0985	0.0011	0.83	681	27	606	6	622	6	97
ZR43	33	315	0.5	0.824	0.01	0.0985	0.0011	0.90	626	25	606	6	610	6	99
ZR12	19	180	0.5	0.879	0.012	0.0985	0.0011	0.81	766	28	606	7	641	7	95
ZR31	22	170	0.9	0.81	0.011	0.0986	0.0011	0.85	589	27	606	7	603	6	101
ZR2	24	214	0.7	0.822	0.01	0.0987	0.0011	0.89	618	25	607	7	609	6	100
ZR16	55	542	0.3	0.847	0.011	0.0992	0.0011	0.89	673	25	609	7	623	6	98
ZR92	17	158	0.4	0.825	0.011	0.0996	0.0011	0.84	607	27	612	6	611	6	100
ZR3	18	146	1.2	0.857	0.011	0.1004	0.0011	0.87	670	26	617	7	628	6	98
ZR14	17	129	1.3	0.844	0.011	0.1006	0.0011	0.85	636	27	618	7	622	6	99
ZR8	99	979	0.3	0.882	0.011	0.1009	0.0011	0.94	722	23	620	7	642	6	97
ZR40	11	79	1.3	0.869	0.014	0.1011	0.0012	0.69	687	34	621	7	635	8	98
ZR33	33	318	0.3	0.864	0.011	0.1025	0.0012	0.90	645	25	629	7	633	6	100
ZR68	118	1214	0.1	0.88	0.01	0.1033	0.0011	0.95	669	23	633	7	641	5	99
ZR79	31	264	0.7	0.87	0.011	0.1035	0.0011	0.87	639	26	635	7	636	6	100
ZR22	17	168	0.2	0.889	0.012	0.1039	0.0012	0.84	676	27	637	7	646	6	99
ZR64	13	121	0.4	0.894	0.012	0.1043	0.0011	0.84	681	27	639	7	649	6	99
ZR58	5	39	1.4	0.873	0.015	0.1043	0.0012	0.65	628	37	640	7	637	8	100
ZR50	39	377	0.1	0.933	0.012	0.1051	0.0012	0.89	755	24	644	7	669	6	96
ZR66	35	305	0.6	0.901	0.011	0.1058	0.0011	0.90	666	24	648	7	652	6	99
ZR35	32	237	1.2	0.894	0.011	0.1063	0.0012	0.89	638	25	651	7	648	6	100
ZR83	40	368	0.3	0.924	0.011	0.1085	0.0012	0.88	667	25	664	7	665	6	100
ZR94	79	692	0.4	0.942	0.011	0.1093	0.0012	0.94	692	23	669	7	674	6	99
ZR84	27	217	0.7	0.95	0.012	0.1094	0.0012	0.85	708	26	669	7	678	6	99
ZR69	23	191	0.5	0.947	0.012	0.1097	0.0012	0.88	695	25	671	7	676	6	99
ZR23	45	419	0.1	0.973	0.012	0.1123	0.0013	0.90	703	25	686	7	690	6	99
ZR96	28	240	0.3	0.981	0.012	0.1143	0.0013	0.91	683	24	697	7	694	6	101
ZR29	9	68	0.6	1.088	0.023	0.1188	0.0014	0.57	821	43	723	8	748	11	97
ZR26	6	37	1.0	1.149	0.019	0.1232	0.0014	0.71	858	33	749	8	777	9	96
ZR10	12	101	0.2	1.14	0.015	0.1256	0.0014	0.85	802	26	763	8	773	7	99
ZR81	7	50	0.4	1.135	0.018	0.1263	0.0014	0.72	781	32	767	8	770	8	100
ZR39	99	756	0.3	1.225	0.014	0.1289	0.0014	0.94	898	22	781	8	812	7	96
ZR44	46	332	0.4	1.233	0.015	0.1328	0.0015	0.92	848	23	804	8	816	7	99
ZR11	9	58	0.5	1.246	0.018	0.1349	0.0015	0.78	838	29	816	9	821	8	99
ZR60	9	60	0.5	1.253	0.018	0.1353	0.0015	0.77	843	29	818	9	825	8	99
ZR27	22	143	0.7	1.244	0.016	0.1357	0.0015	0.86	822	26	820	9	821	7	100
ZR85	92	666	0.3	1.264	0.015	0.1366	0.0015	0.90	841	24	826	8	830	7	100
ZR21	50	338	0.3	1.381	0.017	0.1443	0.0016	0.92	911	23	869	9	881	7	99
ZR34	34	186	0.9	1.498	0.018	0.1548	0.0017	0.93	934	23	928	10	930	7	100
ZR103	56	320	0.6	1.534	0.018	0.1562	0.0017	0.92	965	23	935	10	944	7	99
ZR41	60	345	0.5	1.594	0.019	0.1605	0.0018	0.93	988	22	959	10	968	8	99
ZR89	270	1660	0.7	1.434	0.017	0.1433	0.0016	0.90	1003	23	863	9	903	7	90
ZR102	46	307	0.4	1.402	0.017	0.1399	0.0015	0.89	1005	23	844	9	890	7	89
ZR38	55	297	1.0	1.562	0.019	0.1555	0.0017	0.93	1009	22	932	10	955	7	95
ZR30	56	337	0.2	1.664	0.021	0.1656	0.0019	0.90	1011	23	988	10	995	8	98
ZR18	27	153	0.7	1.581	0.02	0.1569	0.0018	0.88	1017	24	939	10	963	8	95
ZR73	23	126	0.8	1.618	0.021	0.1599	0.0018	0.86	1026	25	956	10	977	8	95
ZR70	31	139	1.2	1.766	0.021	0.1737	0.0019	0.90	1035	23	1032	10	1033	8	100
ZR106	32	147	1.2	1.698	0.021	0.1669	0.0018	0.90	1037	23	995	10	1008	8	97
ZR61	26	150	0.9	1.479	0.021	0.1453	0.0016	0.78	1037	28	874	9	922	9	89

TABLE II. Continued

mpad8	Pb (ppm)	U (ppm)	Th/U	Isotopic Ratios					Apparent Ages						
				$^{207}\text{Pb}/^{235}\text{U}$	1sigAbsErr	$^{206}\text{Pb}/^{238}\text{U}$	1sigAbsErr	rho	$^{207}\text{Pb}/^{206}\text{Pb}$	1sigAbsErr	$^{206}\text{Pb}/^{238}\text{U}$	1sigAbsErr	$^{207}\text{Pb}/^{235}\text{U}$	1sigAbsErr	Conc. (%)
ZR90	80	429	0.4	1.812	0.022	0.1772	0.0019	0.89	1047	23	1051	11	1050	8	100
ZR75	46	212	1.1	1.786	0.021	0.1741	0.0019	0.91	1052	23	1035	10	1040	8	99
ZR80	11	93	0.9	1.019	0.015	0.0994	0.0011	0.74	1052	30	611	7	713	8	68
ZR93	26	128	0.6	1.99	0.025	0.1782	0.0020	0.88	1222	23	1057	11	1112	8	91
ZR6	43	211	0.2	2.367	0.029	0.2075	0.0023	0.92	1263	22	1216	13	1233	9	98
ZR65	283	742	1.0	4.608	0.052	0.3068	0.0033	0.96	1782	19	1725	16	1751	9	99
ZR109	68	178	0.9	4.973	0.059	0.3155	0.0035	0.93	1870	20	1768	17	1815	10	97
ZR100	17	36	1.5	5.354	0.066	0.3376	0.0037	0.90	1881	21	1875	18	1878	11	100
ZR55	443	1571	0.5	4.095	0.048	0.2561	0.0028	0.93	1895	20	1470	14	1653	10	87
ZR104	354	841	1.0	5.641	0.065	0.3405	0.0037	0.95	1959	19	1889	18	1922	10	98
ZR74	86	238	0.5	5.424	0.063	0.3241	0.0035	0.93	1977	20	1810	17	1889	10	96
ZR71	107	237	1.0	6.151	0.07	0.3640	0.0039	0.94	1994	19	2001	19	1998	10	100
ZR5	139	422	0.1	5.57	0.065	0.3270	0.0037	0.96	2008	19	1824	18	1911	10	95
ZR62	82	208	0.4	6.317	0.071	0.3653	0.0039	0.96	2035	19	2007	19	2021	10	99
ZR19	54	126	0.8	6.211	0.074	0.3546	0.0040	0.94	2058	19	1957	19	2006	10	98
ZR15	127	300	0.5	6.879	0.081	0.3829	0.0043	0.96	2102	19	2090	20	2096	10	100
ZR98	320	879	0.2	6.516	0.074	0.3500	0.0038	0.96	2165	18	1935	18	2048	10	95
ZR88	60	132	0.5	7.563	0.092	0.4030	0.0044	0.90	2178	20	2183	20	2181	11	100
ZR110	71	164	0.3	7.617	0.09	0.4007	0.0044	0.93	2201	19	2172	20	2187	11	99
ZR99	45	109	0.4	8.437	0.1	0.3673	0.0041	0.93	2524	19	2017	19	2279	11	90
ZR112	40	104	0.6	7.426	0.092	0.3221	0.0036	0.90	2530	20	1800	18	2164	11	86
ZR9	118	211	1.1	10.022	0.117	0.4265	0.0048	0.96	2562	18	2290	22	2437	11	95
ZR63	435	1038	0.0	9.744	0.108	0.4121	0.0044	0.97	2573	17	2224	20	2411	10	94
ZR51	246	442	0.6	11.308	0.131	0.4756	0.0052	0.95	2582	18	2508	23	2549	11	99
ZR77	207	394	0.5	10.985	0.126	0.4597	0.0050	0.94	2590	18	2438	22	2522	11	97
ZR105	471	980	0.6	9.759	0.112	0.4060	0.0045	0.95	2600	18	2197	20	2412	11	93
ZR53	70	121	0.8	11.22	0.133	0.4628	0.0051	0.93	2614	18	2452	22	2542	11	97
ZR82	141	250	0.7	11.321	0.133	0.4648	0.0050	0.92	2622	18	2461	22	2550	11	97
ZR56	301	719	0.1	9.67	0.114	0.3963	0.0043	0.93	2625	18	2152	20	2404	11	92
ZR86	45	79	0.7	12.084	0.146	0.4811	0.0053	0.90	2673	19	2532	23	2611	11	98
ZR97	226	396	1.1	10.95	0.124	0.4349	0.0048	0.96	2677	17	2328	21	2519	11	94
ZR91	107	184	0.7	12.45	0.141	0.4739	0.0052	0.97	2747	17	2501	23	2639	11	95
ZR49	89	172	0.1	13.302	0.155	0.4819	0.0053	0.95	2828	18	2536	23	2701	11	96

TABLE III.

PC7	Pb (ppm)	U (ppm)	Th/U	Isotopic Ratios					Apparent Ages					Conc. (%)	
				207Pb/235U	1sigAbsErr	206Pb/238U	1sigAbsErr	rho	207Pb/206Pb	1sigAbsErr	206Pb/238U	1sigAbsErr	207Pb/235U	1sigAbsErr	
ZR16	19	206	0.7	0.704	0.009	0.0851	0.0010	0.90	604	25	527	6	541	5	97
ZR20	39	444	0.4	0.708	0.010	0.0853	0.0010	0.84	611	27	528	6	544	6	97
ZR23	94	922	0.9	0.714	0.009	0.0869	0.0010	0.94	591	24	537	6	547	5	98
ZR56	19	209	0.2	0.821	0.012	0.0938	0.0011	0.77	724	30	578	6	608	7	95
ZR3	17	176	0.4	0.796	0.010	0.0942	0.0011	0.90	650	25	580	6	595	6	98
ZR54	34	352	0.3	0.792	0.010	0.0954	0.0011	0.93	612	24	588	6	593	6	99
ZR41	12	107	0.8	0.797	0.012	0.0956	0.0011	0.77	621	31	589	7	595	7	99
ZR74	58	591	0.4	0.821	0.010	0.0966	0.0011	0.92	662	24	595	7	609	6	98
ZR107	34	277	1.2	0.826	0.010	0.0971	0.0011	0.94	664	23	597	7	611	6	98
ZR77	35	365	0.3	0.806	0.010	0.0973	0.0011	0.95	608	23	599	7	600	6	100
ZR32	8	67	1.0	0.809	0.012	0.0974	0.0011	0.75	614	32	599	7	602	7	100
ZR52	17	174	0.2	0.826	0.012	0.0975	0.0011	0.83	656	28	600	7	611	6	98
ZR18	32	319	0.4	0.811	0.010	0.0977	0.0011	0.95	610	23	601	7	603	5	100
ZR27	24	215	0.8	0.811	0.010	0.0977	0.0011	0.92	610	24	601	7	603	6	100
ZR35	23	226	0.4	0.813	0.010	0.0978	0.0011	0.93	615	24	601	7	604	6	100
ZR61	12	109	0.8	0.816	0.011	0.0978	0.0011	0.84	623	27	602	7	606	6	99
ZR8	21	216	0.3	0.828	0.012	0.0979	0.0011	0.82	652	28	602	7	613	6	98
ZR12	50	547	0.0	0.841	0.011	0.0986	0.0011	0.86	671	26	606	7	620	6	98
ZR38	13	121	0.6	0.808	0.010	0.0988	0.0011	0.88	580	26	607	7	602	6	101
ZR72	10	94	0.4	0.836	0.011	0.0991	0.0011	0.84	647	27	609	7	617	6	99
ZR101	17	167	0.4	0.826	0.011	0.0991	0.0011	0.88	619	26	609	7	611	6	100
ZR110	20	189	0.6	0.853	0.011	0.0992	0.0011	0.90	688	25	610	7	627	6	97
ZR51	36	375	0.1	0.841	0.010	0.0995	0.0011	0.95	651	23	611	7	620	6	99
ZR113	8	56	1.6	0.837	0.012	0.0998	0.0012	0.81	632	29	613	7	617	7	99
ZR5	10	97	0.2	0.837	0.011	0.1005	0.0011	0.85	617	27	617	7	617	6	100
ZR13	14	118	1.0	0.843	0.011	0.1007	0.0011	0.85	630	27	619	7	621	6	100
ZR1	5	40	0.7	0.833	0.013	0.1014	0.0012	0.74	587	32	623	7	615	7	101
ZR68	9	79	0.8	0.868	0.012	0.1021	0.0012	0.84	663	27	627	7	635	7	99
ZR75	9	87	0.4	0.873	0.012	0.1023	0.0012	0.84	672	27	628	7	637	7	99
ZR66	32	297	0.4	0.941	0.012	0.1024	0.0012	0.90	827	24	628	7	673	6	93
ZR94	28	277	0.3	0.876	0.011	0.1026	0.0012	0.93	673	24	630	7	639	6	99
ZR79	58	577	0.3	0.863	0.010	0.1027	0.0012	0.97	637	23	630	7	632	6	100
ZR19	38	390	0.1	0.867	0.011	0.1035	0.0012	0.92	630	24	635	7	634	6	100
ZR25	45	429	0.3	0.893	0.011	0.1035	0.0012	0.95	693	23	635	7	648	6	98
ZR43	19	178	0.5	0.863	0.011	0.1035	0.0012	0.91	621	25	635	7	632	6	101
ZR69	29	271	0.4	0.881	0.011	0.1037	0.0012	0.91	660	24	636	7	641	6	99
ZR33	14	131	0.3	1.001	0.014	0.1041	0.0012	0.84	922	26	638	7	704	7	91
ZR71	52	463	0.5	0.903	0.011	0.1047	0.0012	0.93	694	24	642	7	653	6	98
ZR91	22	163	1.0	0.883	0.011	0.1048	0.0012	0.91	645	25	642	7	643	6	100
ZR55	18	153	0.6	0.900	0.011	0.1052	0.0012	0.89	676	25	645	7	652	6	99
ZR90	13	118	0.5	0.926	0.012	0.1060	0.0012	0.86	721	26	649	7	666	7	98
ZR86	29	220	1.1	0.965	0.012	0.1067	0.0012	0.92	794	23	654	7	686	6	95
ZR7	62	560	0.4	0.929	0.011	0.1069	0.0012	0.93	710	24	655	7	667	6	98
ZR102	71	709	0.0	0.923	0.011	0.1071	0.0012	0.93	692	23	656	7	664	6	99
ZR11	15	126	0.6	0.932	0.013	0.1078	0.0012	0.79	698	29	660	7	669	7	99
ZR50	31	298	0.1	0.950	0.012	0.1093	0.0012	0.92	710	24	669	7	678	6	99
ZR34	37	351	0.2	0.945	0.011	0.1095	0.0012	0.94	695	23	670	7	676	6	99
ZR64	12	100	0.6	0.991	0.013	0.1102	0.0013	0.85	782	26	674	7	699	7	96
ZR14	12	104	0.5	0.955	0.014	0.1108	0.0013	0.80	692	29	678	7	681	7	100
ZR53	18	160	0.3	0.963	0.012	0.1130	0.0013	0.92	668	24	690	7	685	6	101
ZR37	16	130	0.5	0.999	0.013	0.1136	0.0013	0.88	734	25	694	8	703	7	99
ZR80	8	68	0.4	1.031	0.014	0.1150	0.0013	0.85	776	26	702	8	720	7	98
ZR109	17	154	0.2	1.004	0.012	0.1163	0.0013	0.92	697	24	709	8	706	6	100
ZR10	60	555	0.0	1.036	0.013	0.1165	0.0013	0.93	758	23	710	8	722	6	98
ZR17	40	337	0.3	1.062	0.013	0.1172	0.0013	0.94	798	23	714	8	735	6	97
ZR45	28	234	0.3	1.025	0.013	0.1183	0.0014	0.92	704	24	721	8	717	6	101
ZR96	13	102	0.6	1.090	0.014	0.1190	0.0014	0.88	821	25	725	8	749	7	97
ZR42	10	64	1.2	1.082	0.016	0.1208	0.0014	0.80	773	28	735	8	744	8	99
ZR67	20	158	0.5	1.069	0.014	0.1210	0.0014	0.89	746	25	736	8	738	7	100
ZR15	23	192	0.3	1.090	0.015	0.1223	0.0014	0.84	762	27	744	8	748	7	99
ZR106	26	198	0.5	1.096	0.013	0.1232	0.0014	0.94	760	23	749	8	752	6	100
ZR93	34	254	0.4	1.231	0.015	0.1247	0.0014	0.92	975	23	757	8	815	7	93
ZR49	18	136	0.5	1.155	0.014	0.1251	0.0014	0.92	836	23	760	8	779	7	98
ZR26	16	123	0.5	1.113	0.015	0.1255	0.0014	0.87	753	26	762	8	760	7	100

TABLE III. Continued

PC7	Pb (ppm)	U (ppm)	Th/U	Isotopic Ratios						Apparent Ages						Conc. (%)
				207Pb/235U	1sigAbsErr	206Pb/238U	1sigAbsErr	rho	207Pb/206Pb	1sigAbsErr	206Pb/238U	1sigAbsErr	207Pb/235U	1sigAbsErr	Conc. (%)	
ZR24	33	249	0.4	1.136	0.013	0.1268	0.0014	0.95	773	23	770	8	771	6	100	
ZR58	12	78	1.1	1.131	0.015	0.1269	0.0015	0.87	762	25	770	8	768	7	100	
ZR85	17	120	0.6	1.179	0.015	0.1298	0.0015	0.91	802	24	787	9	791	7	100	
ZR99	15	111	0.5	1.193	0.015	0.1305	0.0015	0.89	815	24	791	9	797	7	99	
ZR2	42	280	0.7	1.221	0.015	0.1326	0.0015	0.94	832	23	803	8	810	7	99	
ZR78	43	327	0.3	1.201	0.014	0.1329	0.0015	0.96	792	22	804	9	801	7	100	
ZR40	19	141	0.3	1.226	0.016	0.1331	0.0015	0.90	833	24	806	9	813	7	99	
ZR108	31	222	0.4	1.225	0.015	0.1341	0.0015	0.94	814	23	811	9	812	7	100	
ZR44	32	202	0.8	1.262	0.016	0.1349	0.0015	0.92	864	24	816	9	829	7	98	
ZR65	9	66	0.4	1.247	0.017	0.1350	0.0016	0.86	837	26	817	9	822	8	99	
ZR97	11	76	0.3	1.264	0.017	0.1370	0.0016	0.87	836	25	827	9	830	8	100	
ZR95	34	227	0.5	1.281	0.016	0.1384	0.0016	0.94	842	23	836	9	837	7	100	
ZR9	11	73	0.4	1.352	0.018	0.1411	0.0016	0.86	914	25	851	9	868	8	98	
ZR82	32	195	0.8	1.314	0.016	0.1418	0.0016	0.94	844	22	855	9	852	7	100	
ZR92	87	599	0.3	1.353	0.016	0.1421	0.0016	0.96	901	22	857	9	869	7	99	
ZR83	94	627	0.4	1.412	0.017	0.1447	0.0017	0.97	951	21	871	9	894	7	97	
ZR62	31	219	0.2	1.376	0.017	0.1451	0.0017	0.92	893	23	874	9	879	7	99	
ZR4	26	178	0.2	1.401	0.017	0.1470	0.0016	0.92	902	23	884	9	889	7	99	
ZR31	50	304	0.7	1.429	0.017	0.1472	0.0017	0.96	940	22	885	9	901	7	98	
ZR39	31	197	0.3	1.512	0.019	0.1567	0.0018	0.93	927	23	939	10	935	8	100	
ZR28	64	346	0.9	1.532	0.018	0.1572	0.0018	0.97	949	22	941	10	943	7	100	
ZR105	89	395	1.8	1.580	0.019	0.1586	0.0018	0.93	993	22	949	10	962	8	99	
ZR104	46	261	0.6	1.557	0.019	0.1594	0.0018	0.93	954	23	953	10	953	8	100	
ZR70	44	219	1.2	1.582	0.019	0.1595	0.0018	0.93	985	23	954	10	963	8	99	
ZR76	62	363	0.5	1.578	0.019	0.1597	0.0018	0.97	977	21	955	10	962	7	99	
ZR6	59	348	0.4	1.599	0.019	0.1608	0.0018	0.93	989	22	961	10	970	8	99	
ZR47	46	247	0.7	1.612	0.019	0.1633	0.0018	0.94	975	22	975	10	975	8	100	
ZR111	29	169	0.4	1.615	0.019	0.1633	0.0019	0.94	978	22	975	10	976	8	100	
ZR89	28	153	0.6	1.676	0.021	0.1681	0.0019	0.92	995	23	1002	11	999	8	100	
ZR115	27	134	1.0	1.682	0.021	0.1674	0.0019	0.90	1010	24	998	11	1002	8	99	
ZR114	44	247	0.4	1.739	0.021	0.1723	0.0020	0.95	1019	22	1025	11	1023	8	100	
ZR112	16	96	0.6	1.557	0.024	0.1538	0.0018	0.76	1026	29	922	10	953	10	93	
ZR29	28	162	0.7	1.590	0.020	0.1565	0.0018	0.92	1033	23	937	10	966	8	94	
ZR81	12	94	0.9	1.062	0.015	0.1014	0.0012	0.81	1095	27	622	7	735	8	67	
ZR59	41	190	1.3	1.952	0.023	0.1661	0.0019	0.94	1321	21	990	10	1099	8	83	
ZR88	17	108	0.2	2.063	0.025	0.1416	0.0016	0.93	1726	20	854	9	1137	8	66	
ZR22	84	319	0.4	3.649	0.042	0.2448	0.0028	0.98	1769	19	1411	14	1560	9	88	
ZR73	40	284	0.5	1.861	0.024	0.1187	0.0014	0.90	1860	21	723	8	1067	9	57	
ZR46	53	142	0.7	5.056	0.059	0.3222	0.0036	0.97	1862	19	1800	18	1829	10	98	
ZR21	163	563	0.3	4.570	0.052	0.2753	0.0031	0.99	1962	18	1568	16	1744	10	89	
ZR57	74	202	0.5	5.514	0.066	0.3311	0.0038	0.95	1968	19	1844	18	1903	10	97	
ZR87	605	2850	0.2	3.531	0.041	0.2012	0.0023	0.98	2061	18	1182	12	1534	9	74	
ZR60	230	697	0.1	5.744	0.067	0.3258	0.0037	0.97	2069	18	1818	18	1938	10	94	
ZR30	337	911	0.2	6.889	0.080	0.3599	0.0041	0.98	2213	18	1982	19	2097	10	95	
ZR103	314	1278	1.2	3.707	0.045	0.1850	0.0021	0.94	2292	19	1094	11	1573	10	69	
ZR36	178	407	0.1	9.683	0.113	0.4223	0.0048	0.97	2521	18	2271	22	2405	11	95	
ZR84	120	255	0.6	9.293	0.108	0.4042	0.0046	0.98	2525	17	2189	21	2367	11	94	
ZR48	177	389	0.2	10.240	0.117	0.4278	0.0048	0.98	2593	17	2296	22	2457	11	95	
ZR98	174	272	1.4	11.629	0.138	0.4743	0.0054	0.96	2633	18	2502	24	2575	11	98	
ZR100	98	121	2.3	12.429	0.148	0.5047	0.0057	0.95	2640	18	2634	25	2637	11	100	
ZR63	77	139	0.5	12.283	0.145	0.4859	0.0055	0.96	2684	18	2553	24	2626	11	98	

TABLE IV. Operating conditions for the LA-ICP-MS equipment

Laboratory & Sample Preparation	
Laboratory name	GeOHeLiS Analytical Platform, Géosciences Rennes/OSUR, Univ. Rennes
Sample type/mineral	zircon
Sample preparation	Conventional mineral separation, 1 inch resin mount, 1µm polish to finish
Imaging	(CL) imaging using a Quanta 200 SEM with centaurus detector at the Laboratoire Magmas d'océanologie et de géosciences, Université de Lille 1 (Lille, France).
Laser ablation system	
Make, Model & type	ESI NWR193UC, Excimer
Ablation cell	ESI NWR TwoVol2
Laser wavelength	193 nm
Pulse width	< 5 ns
Fluence	7 J/cm ⁻²
Repetition rate	5 Hz
Spot size	25 µm
Sampling mode / pattern	Single spot
Carrier gas	100% He, Ar make-up gas and N ₂ (3 ml/mn) combined using in-house smoothing device
Background collection	20 seconds
Ablation duration	60 seconds
Wash-out delay	15 seconds
Cell carrier gas flow (He)	0.75 l/min
ICP-MS Instrument	
Make, Model & type	Agilent 7700x, Q-ICP-MS
Sample introduction	Via conventional tubing
RF power	1350W
Sampler, skimmer cones	Ni
Extraction lenses	X type
Make-up gas flow (Ar)	0.85 l/min
Detection system	Single collector secondary electron multiplier
Data acquisition protocol	Time-resolved analysis
Scanning mode	Peak hopping, one point per peak
Detector mode	Pulse counting, dead time correction applied, and analog mode when signal intensity > ~ 10 ⁶ cps
Masses measured	²⁰⁴ (Hg + Pb), ²⁰⁶ Pb, ²⁰⁷ Pb, ²⁰⁸ Pb, ²³² Th, ²³⁸ U
Integration time per peak	10-30 ms
Sensitivity / Efficiency	20000 cps/ppm Pb (50µm, 10Hz)
Data Processing	
Gas blank	20 seconds on-peak
Calibration strategy	GJ1 zircon standard used as primary reference material, Plešovice used as secondary reference material (quality control)
Reference Material info	GJ1 (Jackson et al., 2004) Plešovice (Slama et al., 2008)
Data processing package used	GLITTER ® (van Achterbergh et al., 2001)
Quality control / Validation	Plešovice: concordia age = 336.7 ± 0.8 Ma (N=36; MSWD=0.33)

FIGURE I.